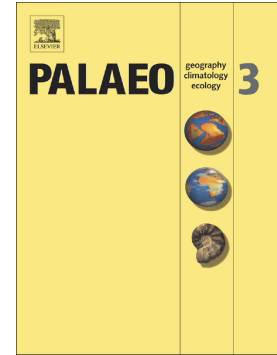


Accepted Manuscript

Coupled stalagmite – Alluvial fan response to the 8.2 ka event and early Holocene palaeoclimate change in Greece

E.N. Peckover, J.E. Andrews, M.R. Leeder, P.J. Rowe, A. Marca, D. Sahy, S. Noble, R. Gawthorpe



PII: S0031-0182(18)31019-8
DOI: <https://doi.org/10.1016/j.palaeo.2019.109252>
Article Number: 109252
Reference: PALAEO 109252
To appear in: *Palaeogeography, Palaeoclimatology, Palaeoecology*
Received date: 13 December 2018
Revised date: 1 May 2019
Accepted date: 25 June 2019

Please cite this article as: E.N. Peckover, J.E. Andrews, M.R. Leeder, et al., Coupled stalagmite – Alluvial fan response to the 8.2 ka event and early Holocene palaeoclimate change in Greece, *Palaeogeography, Palaeoclimatology, Palaeoecology*, <https://doi.org/10.1016/j.palaeo.2019.109252>

This is a PDF file of an unedited manuscript that has been accepted for publication. As a service to our customers we are providing this early version of the manuscript. The manuscript will undergo copyediting, typesetting, and review of the resulting proof before it is published in its final form. Please note that during the production process errors may be discovered which could affect the content, and all legal disclaimers that apply to the journal pertain.

Coupled stalagmite – alluvial fan response to the 8.2 ka event and early Holocene palaeoclimate change in Greece

Peckover, E.N.¹, Andrews, J.E.¹, *, Leeder, M.R.¹, Rowe, P.J.¹, Marca, A.¹, Sahy, D.², Noble, S.², Gawthorpe, R.³.

¹School of Environmental Sciences, University of East Anglia, Norwich NR4 7TJ, UK.

²Geochronology and Tracers Facility, NERC Isotope Geosciences Laboratory, British Geological Survey, Keyworth, Nottingham NG12 5GG, UK.

³Basin and Reservoir Studies Group, Department of Earth Science, University of Bergen, Allegaten 41, 5020 Bergen, Norway.

*Corresponding author email j.andrews@uea.ac.uk

Running header: Terrestrial responses to 8.2 ka palaeoclimate event in Greece

Abstract

We explore the expression of early Holocene climatic change in the terrestrial Mediterranean of southern Greece. A regional palaeoclimate record from stable isotope and trace element geochemical proxies in an early Holocene (~12.4 ka to 6.7 ka) stalagmite is compared to the timing of palaeosol (entisol) development on an early Holocene alluvial fan located less than 100 km from the stalagmite site. Radiocarbon dated entisol development records fan abandonment surfaces, which can be coupled to the stalagmite climate signal. Variations in $\delta^{13}\text{C}$ best record the main elements of palaeoclimatic change, more negative values indicating soil carbon input to karst groundwater under wetter conditions. The wettest conditions begin around 10.3 ka, coincident with the start of sapropel 1 deposition in the eastern Mediterranean. The widely documented northern hemisphere '8.2 ka event' of cooler and drier conditions has a muted $\delta^{18}\text{O}$ climatic signal in common with other stalagmite climate records from the wider Mediterranean. However, less negative $\delta^{13}\text{C}$ values do record a period of episodic dryness between ~8.8 and ending at 8.2 ka. Wetter conditions re-established after

8.1 ka to the end of the record. The oldest alluvial fan entisols were developing by ~9.5 ka, and a prominent rubified entisol developed ~8.3 to 8.4 ka, indicating pedogenesis within dating error of the 8.2 ka event. The speleothem record of episodic dryness between ~8.8 and 8.2 ka, combined with other regional proxies, is consistent with the notion that precipitation patterns in Greece may have changed from predominantly winter frontal to summer convective during this period. Palaeosol formation on the alluvial fan may have been an allocyclic response to this change. It is plausible that fan-channel incision, driven by temporary development of a ‘flashier’ summer rainfall regime, isolated large areas of the fan surface allowing onset of prolonged pedogenesis there.

Keywords: alluvial fan, stalagmite, paleoclimate, Holocene, 8.2 ka event, Greece

1. Introduction

It is a consensus view today that $\sim 8.47 \pm 0.3$ ka, glacial lakes Agassiz and Ojibway released meltwater into the north Atlantic causing surface water freshening (Barber et al. 1999; Clarke et al. 2004; Alley and Ágústsdóttir 2005). The freshening caused slowdown of meridional North Atlantic deep-water flow from c. 8.4 ka, with rapid deceleration and sea-surface temperature reductions at ~8.3 ka (Ellison et al. 2006). The event (“8.2 ka event”) resulted in near global (Cheng et al., 2009) climatic cooling typically accompanied by drier, windier conditions that increased susceptibility to forest fire (Alley et al. 1997). The meltwater pulse that stimulated the 8.2 ka event is the last of up to 17 similar, albeit mostly smaller, pulses identified in the early Holocene (Teller and Leverington 2004). In addition to the 8.2 ka event, at least two more of these melt water pulses are thought to have produced cool and dry climatic anomalies: one at ~9.2 ka (Fleitmann et al., 2008) and the other at ~11.4 ka (the Preboreal Oscillation; Fisher et al., 2002). While all three climatic anomalies register clearly in Greenland ice cores (Vinther et al., 2006) the 8.2 ka event has the best-documented terrestrial climatic expression.

In this study we were interested in understanding the expression of these early Holocene climatic anomalies in the terrestrial Mediterranean, specifically in Greece. We set out to do this by constructing a palaeoclimate record from an early Holocene stalagmite (Figs 1 and 2). Stalagmites are well suited to this approach as they can be precisely dated using U series, while petrographic fabrics, stable isotope and trace element geochemical proxies can record environmental and climatic variability (e.g. Fairchild and Baker 2012).

Despite near-global climatic cooling caused by the “8.2 ka event” its expression is surprisingly patchy, muted or absent in speleothems from wider Mediterranean regions (e.g. Frumkin et al., 1994; Bar Matthews et al. 1999; Zanchetta et al., 2007; Verheyden et al. 2008). It is thus important, where possible, to construct regionally specific, well-resolved speleothem records that provide the best opportunity to attribute climatic effects on regional precipitation, runoff and sediment yields, particularly seasonal distribution, magnitude and source.

We also had an unusual opportunity to compare the local well-dated stalagmite palaeoclimate record with the sedimentary response of an early Holocene alluvial fan located at Schinos, less than 100 km from the stalagmite site (Fig. 1). Radiocarbon chronology for the fan, allowed, perhaps for the first time, quantitative analysis of centennial-scale fan response to climatic drivers, taking such studies beyond the coarser temporal and climatic-change scales seen, for example at the Pleistocene-Holocene transition where dated lake shorelines intersect the distal parts of alluvial fans (e.g. Harvey et al., 1999; Garcia and Stokes 2006).

Our studied fan displays a number of thin palaeosols in its lower part: the thickest and stratigraphically youngest palaeosol having an age of 7620 ± 40 radiocarbon years (Leeder et al., 2002), showing that the fan sediments overlap in age with the early Holocene stalagmite record. Palaeosols in alluvial fan sequences record abandoned surfaces where sedimentation has temporarily ceased (e.g. Talbot and Williams 1979; Ritter et al., 1995; Reheis et al., 1996; Stokes et al., 2007; Ventra and Nichols 2014; Antinao et al., 2016). Such abandonment may arise from *autocyclic* lobe switching when a currently active channel cuts across the fan topographic gradient to jump sideways (avulse) during flood discharge. The new locus of deposition robs sediment supply to the formerly active fan segment (e.g. Ventra and Nichols 2014), allowing pedogenesis on the abandoned surface. Repeated avulsions and lobe abandonment produce a patchwork fan stratigraphic architecture comprising local soil horizons intercalated within alluvium. Our null hypothesis was thus that the fan palaeosols are ‘autocyclic’ being randomly distributed in time and space and not related to climatic drivers as recorded in the stalagmite.

If however, the age of the alluvial fan palaeosols corresponds with climatic events in the speleothem the null hypothesis is challenged. *Alloccyclic* forcing of alluvial fan sedimentation is largely non-random, driven by the sensitivity of the entire catchment-fan system to the

balance between predominant deposition and the non-deposition. This sensitivity often arises through changing hydrology-influenced variables such as seasonal water balance, magnitude and rate of surface and sediment runoff and the density and type of vegetation (Leeder et al. 1998). The commonest signal of allocyclic change is from deposition to erosion, caused by fan channel incision. This promotes development of soil horizons on sediment-starved interfluvial surfaces left stranded above the flooding levels of the incised and eroding channels. Prolonged incision is likely to be driven by climatic changes on centennial or longer timescales and as such, palaeosol development should align with palaeoclimatic events recorded in the stalagmite. Of course, changing gradients caused by (random) tectonic activity and changing base level may also be important, although these are not necessarily a major factor on Quaternary timescales (Ritter et al., 1995).

Our early Holocene stalagmite palaeoclimate record comes from Limnon Cave ($37^{\circ}57'37.8''$ N $22^{\circ}08'24.9''$ E), 2 km north of Kastria village in the Peloponnese, some 90 km SE of Patras (Figs 1 and 2). The climate record spans the first five thousand years of the Early Holocene, broadly between 12 - 7 ka, significantly older than any published speleothem records (e.g. Finné et al., 2015; Weiberg et al., 2016) from the Peloponnese. The stalagmite age thus directly corresponds to dated palaeosol development (Leeder et al., 2002) on the Schinos alluvial fan located in western Attica, some 80 km to the ENE ($38^{\circ}02'53.7''$ N $23^{\circ}02'54.0''$ E; Fig. 1). Most important, the time-period of our study precedes any significant impact from human activity on vegetation in the region, which began around 7.0 ka (Weiberg et al., 2016).

2. Early Holocene climate (Greece)

Central Asian Holocene climate between 10-6 ka was generally warm and humid, linked to onset of the early Holocene (11.5 ka) solar radiation maximum (Cheng et al., 2012). In the Eastern Mediterranean, warm and humid conditions (Peyron et al. 2011; Cheng et al., 2015) coincide with deposition of sapropel 1 (S1; 10.5 ka to 6.1 ka; Grant et al., 2016) a precession minima phenomenon driven by wetter climate, increased river runoff, eutrophication and near-surface stratification (e.g. Mercone et al., 2001; Meyers and Arnaboldi 2008; Rohling et al., 2015). On land, the warm and humid conditions favoured growth of 'climatic optimum' Mediterranean mixed forests. The best-resolved terrestrial palaeoclimate data in Greece comes from Tenaghi Philippon (Peyron et al. 2011) in the north of the country. Here, pollen-

based climate reconstructions show a strongly seasonal (stronger than today) moist period from 9.5-7.8 ka characterised by wet winters and dry summers.

These optimum conditions were interrupted at 9.2 and 8.2 ka (Section 1). The 8.2 ka northern hemisphere climate event is best-documented, dated to 8271 ± 113 years BP (Vinther et al., 2006) based on electrical conductivity measurements in the Greenland GISP2 ice core (see also Thomas et al., 2007). Atmospheric teleconnection from the cooled and freshened N Atlantic surface waters caused expansion of the northern hemisphere polar winter vorticity field (Siberian High; see Renssen et al. 2002; Rohling et al. 2002; Vellinga and Wood 2002). Effects of pan-hemispheric cooling ~8.2 ka (Alley and Ágústsdóttir 2005) included reduced growth rates of Central European oaks (Spurk et al., 2002) and changes to deciduous tree populations (notably *Corylus*; Tinner and Lotter, 2001). Sediment cores in the Aegean Sea record the 8.2 ka event superimposed on a broader same-sign climatic anomaly between 8.8-7.8 ka (Rohling and Pälike 2005; Marino et al. 2009). During this period, Aegean Sea S1 deposition was interrupted as cold winter outbursts from the Siberian High led to surface cooling, renewed deep-water formation and temporary reversion to 'normal' oxygenated hemipelagic deposition (Kotthoff et al. 2008a). Onset of this interruption began at 8.5 ka according to Triantaphyllou et al. (2009). The 8.2 ka climatic anomaly interrupted the otherwise moist conditions and reversed the seasonality (dry winters and wet summers) in pollen records at Tenaghi Philippon (Peyron et al. 2011). However, further south in the Peloponnese, geochemical records in Lake Stymphalia show no clear evidence of environmental perturbation at 8.2 ka (Heymann et al., 2013). From 7.8-5.0 ka, the Tenaghi Philippon terrestrial record suggests lower overall precipitation and reduced seasonality (Peyron et al. 2011) but there are no supporting records from southern Greece.

3. Environmental setting

3.1 Limnon Cave stalagmite

Limnon Cave is hosted in Cretaceous Limestones of Mount Amolinitza (summit at 1420 m). This montane cave is about 2 km long and developed along a NW trending fault. The natural cave entrance is 820 m above sea level, but in 1981, an artificial entrance was opened for tourist access that began in 1990 (Fig. 2). The first prominent stalactite mass is found 80 m from the natural entrance and the cave is actively wet with cave floor lake development 280 m from the natural entrance. There are thirteen cave floor lakes of various sizes in the following 520 m (Iliopouou-Georgudaki and Economidou 1991). Epikarst

thickness increases more or less linearly from the natural entrance to a maximum of 540 m below the summit of Mount Amolinita. Present day terra-rossa soil cover above the cave is thin and patchy, mostly hosted in bedrock fissures. Vegetation is sparse Mediterranean sclerophyllous scrub characterized by *Quercus coccifera* and *Phlomes fruticosa* (Iliopouou-Georgudaki and Economidou 1991).

Today, mean cave air temperature varies between 12.5 °C (winter) and 14.5 °C (summer) with relative humidity between 89% (winter) and 96% (summer; Iliopouou-Georgudaki and Economidou 1991). In summer, air flows in through the entrances and exits via roof fissures with flow velocities of 0.12-0.69 m s⁻¹ (0.5-2.0 m from the cave floor; Iliopouou-Georgudaki and Economidou 1991). This flow reverses in winter. All of these measured environmental parameters are clearly affected by the artificial entrance to some degree and it is reasonable to assume that all of them were either lower (temperature range; air flow) or higher (relative humidity) under natural conditions.

The closest data-rich IAEA and WMO weather stations are both coastal, at Patras (2000-2014) and Athens (combined Hellinikon Airport (1960-1976) and Pendeli (2001-2014) records). Modern rainfall distribution is strongly seasonal with >70% of precipitation falling in autumn and winter months and <20 mm rainfall in summer months. Stalagmite extension and isotopic compositions should thus respond largely to autumn and winter rainfall. In the Limnon region annual rainfall is around 1200 mm per year (Flocas and Giles 1991) with an annual rainfall relative intensity of 3.3 mm/h (between 1962 and 2002), among the highest values in Greece (Kambezidis et al. 2010). Between 65 and 70 % of regional rainfall in the Peloponnese originates from frontal depressions in the winter (Flocas and Giles 1991), such that a summer convective signal, although present (Kambezidis et al. 2010), is not likely to be much represented in stalagmite growth today.

3.2. *Schinos alluvial fans*

Opportunities for observing early Holocene sedimentary successions are rare over much of the Aegean hinterland due to younger sedimentary cover. This holds along the majority of the Corinth rift basin where the entry points of major drainages are marked by depositional Holocene coastlines featuring prograding and aggrading fans. However, the southern active-faulted margin to the Alkyonides Gulf in the easternmost rift is undergoing coastal erosion and is bordered by an incised, hanging-wall coastal bajada. This range front bajada comprises

coalesced sea-cliffed alluvial fans, talus cones, coastal lagoons, marshlands and beach/barrier spit and beach shorelines (Fig. 3; Leeder et al. 1991, 1998, 2002). The alluvial fans are km-scale, coarse grained, stream-flow dominated, fed from drainage catchments located in uplifting footwall-mountains of the Gerania Range with Mesozoic basement comprising limestone, chert, and ophiolitic serpentinites. It is likely that a bajada system has been present here for c. 2 Ma since initiation of the active coastal faults (Leeder et al. 2002). The youngest lowstand bajada was drowned around 7 ka at the Holocene highstand and up to 150 m of coastal retreat may have occurred since. Sea-cliffing of the Holocene alluvial fans began after the 7 ka highstand, amplified by $\sim 1\text{-}2\text{ mm yr}^{-1}$ tectonic subsidence, the fans being in the hangingwall of the active Schinos Fault (Jackson et al., 1982; Collier et al., 1998).

This study concentrates on the early Holocene part of Fan F of Leeder et al. (1998, 2002) where the sea cliff and a roadside quarry allow unusually good access to the lower fan stratigraphy. Fan F has its apex at about 200 m elevation and a basal perimeter of approximately 1.3 km. A single gorge, cut through the limestone range front, fed the fan from a catchment approximately 1 km long and up to 0.6 km wide (700 m maximum elevation). The fan surface is densely wooded except parts of the western lower slopes, which have been cleared for house building. We estimate Fan F to have a present day volume of $4.76 \times 10^7\text{ m}^3$, and using a sediment bulk density of 1520 kg m^{-3} , a sedimentary mass of $\sim 7.24 \times 10^{10}\text{ kg}$. Fan F currently shows no evidence of active channel sedimentation; this reflects exhaustion of readily erodible ophiolite, combined with exposure of underlying limestone bedrock in the upper catchment, inducing subsurface (karst) drainage. The youngest ages, presented in Section 5.2, suggest that the eastern part of Fan F may have been largely inactive since the mid Holocene.

Fan F is located in the hangingwall of both the Schinos and Pisia Faults (Jackson et al., 1982; Collier et al., 1998), and the footwall of the offshore West Alkyonides Fault. However, late Quaternary displacements were dominated by subsidence in the hanging walls of the onshore faults (Leeder et al., 2002; Mechernich et al., 2018). The effects of individual earthquakes on fan morphology are well constrained by research on Fan D, 2 km to the E of our study site. In 1981 a series of three earthquakes (February 24, 1981, 6.7 M_s ; February 25, 1981, 6.4 M_s ; March 4, 1981, 6.4 M_s) struck the Alkyonides Basin (Jackson et al., 1982). On Fan D, surface displacements of between 0.4-1.3 m on the Schinos Fault were recorded, probably formed by one or both of the first two 1981 events (Collier et al., 1998). A maximum recurrence interval of 330 years for such surface breaks has been calculated based

on dated historical events (Collier et al., 1998). The presence of a 5 m high scarp on Fan G (~2.5 km SW of our study site) led Collier et al. (1998) to conclude that rates of displacement may be comparable along much of the length of the Schinos Fault, since at least the mid-Holocene. These well-characterised alluvial sediment-hosted fault scarps have surprisingly little effect on overall fan morphology (particularly in the lower fans): in active channel areas they are rapidly degraded/overridden by flood sedimentation events. In short, there is no evidence that individual fault surface scarps have much discernible influence on wider fan sedimentation patterns downslope.

4. Materials and methods

4.1. Limnon Cave

Stalagmite KTR-2, was collected about 600 m from the natural entrance (Fig. 2) where epikarst thickness is about 200 m. Cave water samples (Table S1) were collected at the time of sampling and in addition two drip sites (1 and 2) were subsequently monitored in December 2006 and January 2007, February, March and April 2009, and February and March 2010. Two modern calcite-water pairs were sampled: (1) a small active stalagmite (KTR-1, 400 m from the natural entrance (Fig. 2) growing beneath drip 1 and (2), a nearby straw stalactite (drip 2). The tip of a stalactite drape at 550 m and calcite precipitating on the steel walkway at 500 m was also sampled (Table 1). In addition, water samples from three springs were collected, one 200 m from the natural cave entrance, a second 2 km N of the cave (972 m elevation) and a third at Kalavryta, 17 km NNW of the cave (795 m elevation).

U-Series dating was carried out at the NERC Isotope Geosciences Laboratory, Keyworth, UK (full method in Supplementary Information) using 200-250 mg samples from drilled locations (Fig. 2). Uranium and thorium isotope data were obtained on a Thermo Neptune Plus MC-ICP-MS using an Aridus II desolvating nebulizer and standard-sample bracketing and instrument procedures modified from Andersen et al. (2008) and Hiess et al. (2012). Hydride and tailing corrections were on the order of 2 ppm of the adjacent peaks. Total ^{238}U and ^{232}Th blanks were <10 pg and <4 pg and were negligible relative to the sample U and Th. Standard accuracy (within 0.1%) and reproducibility (within 0.2%) of $^{234}\text{U}/^{238}\text{U}$ was monitored by replicate analyses of Harwell uraninite HU-1. Replicate measurements of the reference solution showed $^{229}\text{Th}/^{230}\text{Th}$ accuracy and reproducibility to be $\pm 0.2\text{-}0.3\%$ for ^{230}Th ion beams > 5000 cps. Data reduction incorporated the revised average $^{235}\text{U}/^{238}\text{U}$ ratio of 137.818 (Hiess et al., 2012) and U-Th ages were calculated using the decay constants of

Cheng et al. (2013). Holocene U/Th ages have errors $< \pm 82$ years (Table 2) and corrected ages are BP (before 1950 AD).

Petrography on KTR-2 was done using multiple overlapping thin-sections and samples for stable isotope analysis were drilled at 1 mm spacing through the axial part of the stalagmite (127 samples; hereafter low-resolution). In addition, a 33 mm section between 33 and 66 mm, was micro-milled at high-resolution in an attempt to capture details of any 8.2 ka signal. Samples were drilled in trenches ~ 250 μm wide and ~ 100 μm deep, normal to the growth axis. Each sample 'sweep' abutted the preceding one such that sample trenches were quasi continuous along the growth axis. This sampling achieved decadal resolution based on the age model. Isotopic analyses (University of East Anglia Stable Isotope Laboratory) were made on 75 ± 5 μg samples, run alongside 75 ± 5 μg internal standards of UEACMST (University of East Anglia Carrara Marble Standard; $\delta^{18}\text{O}$ -2.05 ‰VPDB; $\delta^{13}\text{C}$ 1.99 ‰VPDB), reacted with 105% ($\rho = 1.92$ gml⁻³) phosphoric acid (H_3PO_4) at 90°C in an on-line common acid bath. The evolved CO_2 was purified and analysed for $\delta^{18}\text{O}$ and $\delta^{13}\text{C}$ using a Europa SIRA II dual inlet isotope ratio mass spectrometer. The data are calibrated to international reference scales (VPDB and VSMOW) using IAEA Certified Reference Material NBS-19 ($\delta^{18}\text{O}$ -2.20 ‰VPDB; $\delta^{13}\text{C}$ 1.95 ‰VPDB). Repeat analysis of both international and internal reference materials gave 1σ errors of less than ± 0.1 ‰ for both $\delta^{18}\text{O}$ and $\delta^{13}\text{C}$.

A tablet immediately adjacent to the micromilled section was used for laser ablation ICPMS trace element transect, using a spot size of 30 μm and increment between spots of 200 μm (method in Royle et al., 2015). Sr and Mg data were highly reproducible with RSDs of 2.8% and 3.8% respectively. Exact matching of micro-milled samples and LA-ICPMS spots was not possible due to the poor optics of the laser microscope and the destructive style of drilling, but sample widths of both techniques were close enough to ensure that decadal-scale sampling coherence was achieved.

4.2. Alluvial fan palaeosols

The alluvial fan studies focus on the palaeosols and associated sediments in the basal 10 m of the Schinos bajada alluvial fan F of Leeder et al. (1998, 2002); field colours were recorded with reference to Munsell colour chips. Samples for radiocarbon analysis were taken from the upper few centimetres of the palaeosols, excavated >5 cm behind pre-cleaned

vertical surface exposures, taking great care to avoid modern root material. Bulk sediment was processed by Beta Analytic and the AMS dated material is the organic fraction remaining after sieving the sediment to $<180\ \mu\text{m}$ to remove any roots or macrofossils and then acid washed to remove carbonate. The organic component in these oxic sediments is assumed to be finely-disseminated inert micro-charcoal, accumulated as a concentrate from wildfires. Radiocarbon dates have errors $< \pm 40$ years and were converted to calibrated age ranges BP (before 1950 AD) using INTCAL 13 (Reimer et al. 2013; Table 2).

5. Results

5.1. Limnon Cave stalagmite

KTR-2 is a twin stalagmite; we sampled the left hand stalagmite shown in Figure 2 and nine U-series dates were used to constrain ages (Table 2). The two lower dates bracket a detritus-rich horizon ~ 2 mm in width, which lies at or just below the Pleistocene-Holocene boundary (top at 127 mm). The data show evidence of slight detrital contamination (most $^{230}\text{Th}/^{232}\text{Th}$ being in the range 100-310) and ages have been corrected assuming a contaminant of bulk Earth composition with a Th/U weight ratio of 3.8 (Taylor and McLennan 1995) and ^{238}U , ^{234}U and ^{230}Th in secular equilibrium. Age corrections are generally ≤ 100 years, although ~ 160 years for KTR2-2 and KTR2-3. The dates are in stratigraphic order except KTR2-5 and KTR2-6 with an age differential of 180 years, and stratigraphically inverted beyond 2σ errors: there are no obvious geochemical grounds to prefer one date over the other (Table 2). KTR2-5 (8641 ± 43 years BP) has a lower $^{234}\text{U}/^{238}\text{U}$ ratio than all other samples, possibly indicating uranium isotope mobility, but KTR2-6 (8821 ± 50 years BP) may have experienced detrital contamination by sediment with lower Th/U ratio than bulk Earth leading to higher ^{230}Th and increased age. The speleothem age modelling program StalAge (Scholz and Hoffmann, 2011), rejected sample KTR2-5; however, this solution requires an implausible 10.2 mm of stalagmite extension in 3 years between 61.82 to 72.0 mm. On this basis we think it likely that KTR2-5 is the more reliable age and it was incorporated into the StalAge model used for subsequent data interpretation (Fig. 4).

An age model that includes KTR2-5 but excludes KTR2-6 modifies ages by < 50 years relative to the opposite selection, except between 8.5 ka and 9.0 ka where ages differ by up to 270 years at 8.9 ka (Fig. S1). However, the magnitude of the variation between the two model

chronologies is insufficient to have a significant impact on the palaeoclimatic reconstructions discussed in this paper. The dates shows that speleothem growth above the basal detritus-rich horizon began ~12.4 ka and continued until ~6.7 ka. There is only one likely minor hiatus (at 96 mm), indicating largely continuous extension. Stalagmite extension rates began ~1.1 cm ka⁻¹ between 12.4 ka and 8.9 ka increasing to ~8.4 cm ka⁻¹ between 8.9 ka and ~8.5 ka before falling to ~2.9 cm ka⁻¹ from ~8.5 ka to 6.7 ka (Fig. 4).

Petrography shows that KTR-2 is wholly calcitic mostly of columnar open (Co) fabric (Frisia 2015) with patchy horizons of columnar microcrystalline (Cm) fabrics (Frisia 2015) seen below 60 mm, particularly at 115 and 96 mm (Figs 5a, b). Cm fabrics are in places accompanied by irregular calcite crystals that grew laterally toward the speleothem flank, e.g. at 31 mm (Fig. 5c) and marked by a sub-mm black horizon in hand specimen. The horizon at 96 mm contains the only evidence of clay-rich detritus as a layer that truncates lateral crystal growth (Fig. 5d). The top 2 mm of the stalagmite shows evidence of post-growth corrosion.

The most instructive isotopic and trace element data are shown in Figures 6-8, with additional data and figures available in the Supplementary Information. The $\delta^{18}\text{O}$ record (Fig. 6a) begins with values around -6.5‰ with low variability until ~8.8 ka, after which $\delta^{18}\text{O}$ generally increases to around -6.2‰ . Superimposed on this are ~1‰ negative excursions at 8.5 and 8.0 ka, interspersed with a positive excursion centred on 8.2 ka and most clearly seen in the micro-milled data (Fig. 7a). Another marked positive shift occurs at 7.0 ka (~1.4‰) prior to termination of growth. $\delta^{13}\text{C}$ fluctuates around -5.5‰ before 10.3 ka and mostly between -6.0 to -8.0‰ thereafter (Fig. 6b). However, variability in $\delta^{13}\text{C}$ is high throughout, and a period of less negative values between -5.5 and -6.0‰ , is evident between ~8.8 and 8.1 ka (Figs 6b and 7b): even in this period there is a negative excursion at ~8.5 ka. Excursions to less negative $\delta^{13}\text{C}$ are clear in the micro-milled record at 8.3 ka and between 8.2 and 8.1 ka (Fig. 7b), the latter coincident with the highest $\delta^{18}\text{O}$ value. A major positive excursion at the end of the record matches that in $\delta^{18}\text{O}$.

There is no obvious relationship between variation in high-resolution $\delta^{13}\text{C}$ and any trace element (Figs S3-S5). However, the smoothed high-resolution $\delta^{18}\text{O}$ (Fig. S2) shows some similarity (within dating error) to variability in molar Mg/Sr (Fig. 8), a parameter where variability suggests a mixed control on one or both elements (Tremaine and Froelich 2013) through epikarst processes or source effects (Roberts et al., 1999; Fairchild et al., 2000), including residence times and degassing / prior precipitation (see Brasier et al., 2010). There is also weak relationship between Mg/Ca (and Sr/Ca) vs $\delta^{18}\text{O}$ profile shape, particularly the

first 200 years of the record (Fig. 8) and again from ~8.3 ka to the end of the record at 6.7 ka. Mg/Ca generally increases from ~8.4 ka to ~8.1 ka but with a marked reversal near the 8.2 ka peak in $\delta^{18}\text{O}$ (-6.2 ‰): Mg/Sr (and Sr/Ca) show a substantial increase at this point (Fig. 8).

5.2. Alluvial fan palaeosols

The sea-cliffed fans have vertical faces up to 9 m high that expose crudely-stratified, dm-m thick, lenticular-bedded, open framework gravels that are grain-supported, comprising subangular to subrounded serpentinite/limestone clasts (Fig. 9a and b). The lenticular-bedded gravel units are in places accentuated by intercalated pale-coloured (2.5Y 8/2) fine silt of serpentinite composition (checked by XRD), probably reworked by water flow downslope since the silt has intercalated sand and granule stringers and is often cut out laterally by dm-scale erosional scours hosting coarser sediment (Fig. 9b). Intercalated palaeosols (Fig. 9a and b) range from centimetric- to decimetric-thick, brownish to red (see Munsell colours below) iron-oxide stained horizons that partition the alluvial sediments into successive units (Fig. 10). The INTCAL 13 calibrated ages of the palaeosols are shown in Table 3 and on Figures 9-11. Palaeosol dates are mean residence time (MRT) ages, the average age of the organic carbon component in the sample. MRT ages are typically older than the age of the latest soil development and can suffer from reworking of older material into the soil (Collier et al., 1998). We thus consider the palaeosol ages as maxima and accept that the real age of the soils could be younger. Likewise, MRT ages on silt layers will suffer incorporation of older material into the sediment during deposition and are thus likely to be older than the depositional age. This said, the overall stratigraphic consistency of the ages suggest they are representative.

The oldest lower fan sediments crop out at modern sea-level in a 4.4 m high sea cliff (38°03' 10.1" N 23°03' 08.6"; Figs 9 and 10). The oldest sediments here are streamflow alluvium with a thin, irregular, mottled pale brown - brown (2.5Y 8/2 and 7.5YR 5/4) coloured palaeosol, dated to 9.3 - 9.5 ka (sample JEA140916-3; Table 3). The 2.95 m thick gravel unit overlying this basal palaeosol is particularly rich in limestone clasts, its upper part punctuated by an erosion surface of prominent clasts with low matrix content. Above this is a prominent, laterally continuous palaeosol, 30 cm thick, that weathers light red (10R 6/8) in its upper part. The sample from this palaeosol gave an age of 9.5-9.7 ka (sample JEA140916-5; Figs 9-10). The age is thus apparently the same or older than the underlying palaeosol, the

degree of inversion depending on the calibration age range chosen, and may be indicative of inaccuracies with MRT ages.

This prominent palaeosol is sharply overlain by a silty lens up to 20 cm thick which returned an age of ~7.8 to 7.9 ka (sample JEA140916-4; Table 3 and Figs 9 and 10). Both the silts and the palaeosol are locally cut-out by erosional scour surfaces. The silts are in turn overlain by 60 cm of pebbly gravels topped by a weakly developed, 5 cm thick palaeosol (not dated) overlain sharply by another 10 cm thick silt layer. This silty layer is also cut out locally by gutter-like erosional scours (Fig. 9b). The upper cliff section comprises c. 5 m of streamflow gravels (Fig. 10) with a thin, discontinuous, yellowish red (5YR 5/6) palaeosol at the top which returned an age of 4.9 -5.3 ka (sample JEA140916-6; Table 3). This palaeosol underlies a gravel lens that thickens eastward.

An east-west quarry section at about 7 m elevation (38°03' 05.7" N 23°03' 15.8"; Figs 10 and 11), 250 m SE of the seacliff section features a striking 0.3 m thick laterally-continuous, iron-oxide stained (red; 10R 5/8) palaeosol which caps a >2 m thickness (base not seen) of streamflow alluvium (Figs 10 and 11a). It is itself overlain by c. 6 m of serpentinite-rich alluvial gravels. The palaeosol here comprises light-red (10R 6/8) surface coats to serpentinite clasts and clay/silt-matrix in its upper 10 cm, with rubification decreasing downwards to more red-brown (10R 4/6 to 2.5YR 4/6) hues. There is no evidence of organic horizons or rootlets. Excepting the clay/silt development and colour changes with depth, there is no evidence of marked horizonation in this (or any of the other) palaeosols; the topmost few cm were sampled (MRL109914-5; Table 3 and Fig. 11b) returning an age of 8.3 to 8.4 ka. Overlying streamflow gravels have a sharp and sometimes erosive contact with the palaeosol (Fig. 11b). Sample MRL090911-4A (Table 3) was from a pale coloured (2.5Y 8/2), poorly-sorted sandy-granuley coarse silt in an irregular lens-shaped unit, in the base of the post-palaeosol alluvium, 10 cm above the top of the 8.3 to 8.4 ka palaeosol (Fig.11b). This sample returned an age of 5.0-5.3 ka (Table 3). The silt layer is overlain by 60 cm of gravel, followed by a second 10 cm thick silty layer, locally cut by erosional scours that in places also cut through the underlying gravels and the palaeosol.

6. Interpretation of results

6.1. Stable isotopes background

Isotopic compositions of IAEA Patras precipitation augmented with OIPC v3.1 interpolated precipitation values for the Limnon Cave region (www.waterisotopes.org; Bowen and Wilkinson 2002; Bowen and Revenaugh 2003) mostly plot on, or just above, the GMWL (Fig. S6) while modern cave drip and pool waters, and nearby spring waters (Table S1) plot midway between the GMWL and the EMMWL, with similar gradient. Winter precipitation in the Peloponnese is typically ~ 4 ‰ more negative in $\delta^{18}\text{O}$ than summer precipitation (Fig. S6; the difference can be ~ 6 ‰ when including isotopically enriched Patras/Athens August values). Weak correlation between modern Patras air temperature and rainfall $\delta^{18}\text{O}$, but strong anti-correlation ($r^2 = 0.80$) between mean monthly rainfall amount and mean rainfall $\delta^{18}\text{O}$ (Fig. S7) suggests that the amount effect is largely responsible for the negative winter precipitation $\delta^{18}\text{O}$, as noted in other Mediterranean region palaeoclimate records (Bard et al., 2002, Bar-Matthews et al. 2003, Drysdale et al., 2009, Finné et al., 2014). The modern cave water $\delta^{18}\text{O}$ overlap the four most negative (December-March) OIPC, which overall suggests a mixed Atlantic and Mediterranean moisture source, with recharge predominantly during autumn and winter. The two spring waters sampled >2 km from the cave have more negative $\delta^{18}\text{O}$ than the cave waters, caused by orographic effects of recharge at higher altitude; they do however, help define the local meteoric line and its identical slope to the EMMWL (Fig. S6).

Limnon cave water samples have a mean $\delta^{18}\text{O}$ of -7.50 ± 0.12 ‰ VSMOW. Excluding the slightly enriched drip 1 sample of January 2007 (-7.1 ‰), the average is -7.52 ± 0.06 ‰ VSMOW ($n=17$). Considerable isotopic homogeneity is therefore evident, suggesting effective groundwater mixing in the epikarst.

The extent to which oxygen isotopic equilibrium is maintained during precipitation of speleothem calcite from parent seepage water has typically been evaluated using the equilibrium fractionation equation of Kim and O'Neil (1997) derived from laboratory precipitation experiments (but see Daëron et al., 2019). The calculated temperatures can then be compared with measured cave temperatures. However, extensive investigation of empirical speleothem and cave water oxygen isotope data (Tremaine et al., 2011) suggests that natural carbonate-water isotopic systems may not be well-reproduced by laboratory experiments. The best-fit "cave calcite" line through a plot of the available global speleothem-water $\delta^{18}\text{O}$ data is described by the equation:

$$1000\ln\alpha = 16.1 (10^3\text{T}^{-1}) - 24.6 \quad (1)$$

suggesting that water-calcite equilibrium fractionation factors are likely higher in natural cave systems (see also Daëron et al., 2019) than in laboratory experiments,

Air temperatures at the sample points varied between 12.5- 13.3 °C (RH 89-90%) in winter and 14.2 °C to 14.5 °C (RH of 96%) in summer (Iliopouou-Georgudaki and Economidou, 1991), and a spot reading during sampling in November 2006 was 14.5 °C. Winter pool water temperatures in this part of the cave are between 12-13 °C (Iliopouou-Georgudaki and Economidou, 1991). The mean annual temperature at Tripoli, 50 km SE of the cave is 14.1 °C (1961-1990; altitude 650 masl) and mean annual temperature at Kalavryta (10 kms NNW, 731 masl) is 13.6°C (Pope et al., 2017), the equivalent temperature at the cave site (850 masl) being ~12.8°C. Cave temperatures are thus within ± 1.8 °C of the local annual average temperature. Under wet winter – dry summer Mediterranean conditions calcite precipitation may occur predominantly in winter and therefore calculated cave temperatures of around 12°C are expected. Calculated temperatures using the Tremaine et al. (2011) equation are shown in (Table 1) which also shows the Kim and O’Neil (1997) temperatures for comparison. The modern calcite calculated temperatures fall within the expected range (12.6°C and 13.1°C) excepting the deposit on the metal walkway which appears anomalous (see Supplementary Information). These data show that most modern Limnon Cave speleothem calcite is forming in near-equilibrium with its winter drip waters. We assume these conditions largely held during the early Holocene, and in support of this the petrographic fabrics in KTR-2 (Section 6.2) also suggest low degassing efficiency.

6.2. KTR-2 record

The columnar open (Co) fabrics seen in most of KTR-2 typically form under constant and relatively high drip rate (0.1- 0.3 ml/min; Frisia et al., 2000; Boch et al. 2011) and in a thicker water film than columnar compact calcites. Under these conditions, degassing is less efficient (Kendall and Broughton 1978; Boch et al. 2011) which discourages complete coalescence of crystallites. Co calcites typically form in dripwater with Mg/Ca ratios < 0.3 and pH from 7.4 to 8.0 (Boch et al., 2011), the resulting high HCO_3/CO_3 ratios promoting vertical linear extension. Columnar microcrystalline (Cm) fabrics form under more variable drip rates (30 ml to < 0.1 ml/min; Frisia and Borsato 2010) but most importantly with clear input of impurities and organic colloids when compared to Co conditions (Frisia 2015); the highly irregular crystal boundaries, typical of Cm fabrics, form where foreign particles induce crystal defects (Frisia et al. 2000). In Alpine settings, typically with mixed conifer and

deciduous forest cover, combination of low dripwater supersaturation, low degassing and increased flushing of colloidal particles appears to occur in autumn (Frisia et al., 2005) and suggests that Cm is indicative of seasonal temperature and rainfall (increase in autumn) contrast. Seasonal change in cave ventilation may also be indicated with less efficient exchange between cave and atmospheric air occurring when inflow of soil-derived colloidal particles is greater (Frisia 2015).

The association of Cm fabrics with irregular lateral crystal growth toward the stalagmite flank in KTR-2, may indicate growth in very thin water films (and thus low drip rates at these times), precluding substantial vertical extension.

Much of the Holocene growth of KTR-2 and its subsequent cessation is coincident with the timing of S1 in the Eastern Mediterranean (Section 2) with conditions at this time broadly wetter and warmer than the rest of the Holocene. Wetter conditions than present are borne out by KTR-2 $\delta^{18}\text{O}$, which are typically up to 0.5‰ more negative than modern speleothem calcite values. KTR-2 $\delta^{13}\text{C}$ values are nearly all less negative (typically by 1.5 – 2.0‰) than the mean modern speleothem calcite value of -8.3‰ (Table 1), and this is particularly marked in the earliest part of the record until 10.3 ka (Fig. 12). These ‘high’ $\delta^{13}\text{C}$ values suggest less input of isotopically negative soil-carbon relative to today, particularly in the period before 10.3 ka. Cool conditions evident in the Adriatic from 11.0 ka to 10.0 ka (Rohling et al. 1997), and as late as ~9.6 ka in the Northern Aegean (Gogou et al. 2007; Fig. 12) may have limited soil development, particularly if accompanied by summer aridity (see e.g. Heymann et al., 2013). Petrographic fabrics between 11.2 ka and 9.4 ka alternated between Co and Cm, suggesting short periods of constant drip water supply (Co) giving way to periods of more variable drip rate (Cm). KTR-2 Holocene extensions rates were mostly at their lowest during this period, ~1.1 cm ka⁻¹, until 8.9 ka (Fig. 4). There is no clear evidence of the Preboreal Oscillation climatic anomaly (cold and dry) between 11.4-11.2 ka excepting the possibility that it could have contributed to a ‘high’ in $\delta^{13}\text{C}$ (Fig. 12) at this time.

At ~10.3 ka there is a sharp 3‰ decrease in $\delta^{13}\text{C}$ (to -7.8‰; Fig. 12), heralding a period of ~1000 years when $\delta^{13}\text{C}$ remained below -7.0‰ and indicating increased input of isotopically negative soil-carbon, not dissimilar to present day conditions. During this same 1000 years $\delta^{18}\text{O}$ is <-6.7‰, the most sustained period of isotopically light compositions in the Holocene record and indicative of increased winter rainfall with an intensified ‘amount effect’. These ‘warm and wet’ indicators that promoted biologically active soils, coincide

with the start of S1 (Grant et al., 2016) and the onset of a Holocene Climate Optimum. In this interval Cm fabrics underlie a detritus-rich layer at 96 mm, ~9.4 ka (Fig. 5d) suggesting at least one period (~200 years based on layer width) when infiltration was capable of transporting soil-derived colloids and particles through conduits. The $\delta^{13}\text{C}$ record suggests optimum conditions ended at ~8.8 ka in KTR-2 (Fig. 12) when values increased markedly indicating drier conditions.

The early KTR-2 'optimum' is broadly coincident with a number of regional terrestrial and marine palaeoclimate indicators. The largest and most rapid increase in early Holocene Aegean sea surface temperatures occurred between 10.0 and 9.0 ka (Triantaphyllou et al., 2016), combined with pulsed input of terrestrial organics (Gogou et al. 2007) and lowering of surface salinity, caused by increased fluvial discharge (Kotthoff et al. 2008b). Onset of Aegean and Ionian sapropel formation occurred ~9.8 ka (Gogou et al., 2007; Kotthoff et al., 2008b; Geraga et al., 2008) following the period of most negative $\delta^{13}\text{C}$ values in KTR-2. At Tenaghi Philippon and Nisi Fen (N. Greece) terrestrial pollen data indicates increased winter precipitation and stable winter temperatures between 10.4 ka and 9.5 ka (Kotthoff et al. 2008a), the younger age within error of the ~9.4 ka detritus-rich layer in KTR-2. There is no convincing expression of a 9.2 ka cold and dry climatic anomaly (Fleitmann et al., 2008) in the KTR-2 record.

Between ~8.8 and 8.2 ka, $\delta^{18}\text{O}$ values are typically around -6.6 to -6.5‰ (Fig. 12) while $\delta^{13}\text{C}$ increase to $\sim -6.6\text{‰}$, values broadly similar to those before 10.3 ka, suggesting a return to decreased winter rainfall and re-established dryness. These timings correspond to regional climatic deterioration (aridity) that began around 8.8 ka (Rohling and Pälike 2005; Marino et al. 2009) culminating in the northern hemisphere '8.2 ka event' of cooler and drier conditions centred between 8.2 and 8.1 ka (Alley et al. 1997). However, a ~200 year negative excursion in both isotopes ~8.5 ka in KTR-2 is a clear exception in this trend, the possible significance of which is discussed later.

High-resolution $\delta^{18}\text{O}$ (micro-milled profile) between 8.6 ka to 8.4 ka decrease to a minimum of -7.5‰ between 8.5 and 8.4 ka (Figs 7a and 13) accompanied by negative $\delta^{13}\text{C}$ and peaks in Sr, Ba, Na and P content (Fig. S4): stalagmite extension rates were also at their highest, $\sim 8.4 \text{ cm ka}^{-1}$ sometime between 8.9 ka and 8.5 ka (Fig. 4). The combined information suggest significant rainfall infiltration ($\delta^{18}\text{O}$) that mobilised soil-based lithogenic

colloids and soil organic matter (trace element and $\delta^{13}\text{C}$ response). However, from 8.4 ka, $\delta^{18}\text{O}$ progressively increases to a maximum of -6.2‰ at ~ 8.2 ka (Figs 7a and 12), while $\delta^{13}\text{C}$ shows two more low negative ($>-6.0\text{‰}$) excursions ~ 8.3 ka and ~ 8.2 ka. These isotopic trends are accompanied by increasing Mg/Ca (but with a reversal that matches the timing of the ~ 8.2 ka low negative $\delta^{13}\text{C}$) and a peak in Mg/Sr ratio ~ 8.2 ka (Fig. 8). The combined data are indicative of increasing dryness ($\delta^{18}\text{O}$), possibly associated with a change in moisture source, and increasing water residence time in the epikarst ($\delta^{13}\text{C}$, Mg and to a lesser extent Sr), possibly accompanied by prior calcite precipitation (PCP). The overall $\delta^{13}\text{C}$ response between 8.6 and 8.2 ka is clearly not one of progressive change; instead, it shows marked 1‰ fluctuations around a value of -6.0‰ , changing to lighter compositions after 8.1 ka (Fig. 12). The $\delta^{13}\text{C}$ values while thus relatively high and broadly consistent with episodic dryness, are mostly not as high as values attained in the period before 10.3 ka (Fig. 6b). This suggests aridity was not as marked as in the early Holocene and is supported by development of more open columnar calcite (after 9.2 ka) indicating more consistent recharge and steady infiltration. KTR-2 extension rates had slowed $\sim 2.9\text{ cm ka}^{-1}$ after 8.5 ka (Fig. 4). Cm fabrics are not present after 8.6 ka (Fig. 7a) suggesting drip rate was reasonably constant from this time onward.

The developing dryness recorded in KTR-2 between ~ 8.4 and 8.2 ka (Fig. 7) is consistent with growing evidence that the ‘8.2 ka event’ is superimposed on a climatic deterioration trend between 8.8 ka to 7.8 ka (Rohling and Pälike 2005). The KTR-2 dryness is also consistent with lower resolution chronologies for the onset of water level reduction in nearby Lake Stymphalia (Fig. 1; Heymann et al. 2013) and in the southern Balkans and Macedonia (lakes Maliq and Dojran; Bordon et al. 2009; Francke et al. 2013). The combined ‘peak dryness’ indicators in KTR-2, ~ 8.2 ka, are all within error of the timing of minimum tree pollen percentages at Tenaghi Philippon in N Greece (Peyron et al. 2011) and within error of lake level low-stand ~ 8.2 ka at Stymphalia (Fig. 1; Heymann et al. 2013). In marine records an increase in Ionian Sea surface salinity occurs around ~ 8.0 ka (Emeis et al. 2000) and disruption of Aegean S1 closest to the Greek coastline occurs between 8.4 and 8.0 ka (Kotthoff et al. 2008b).

After 8.1 ka both $\delta^{18}\text{O}$ and $\delta^{13}\text{C}$ become progressively more negative (Fig. 13) and Mg/Ca and Mg/Sr ratios decrease (Fig. 8), all consistent with renewed increase in precipitation as ‘optimum conditions’ re-established. While the apparently ‘wetter’ $\delta^{18}\text{O}$

signature is short-lived (~400 years until ~7.7 ka) the $\delta^{13}\text{C}$ values, fluctuate between -6 and -8‰ until ~7.0 ka (Fig. 6b). The $\delta^{13}\text{C}$ response suggests there was usually enough rainfall to support vegetation during this period, perhaps because of effective summer rainfall, or if temperatures were cool (solar insolation being in decline at this time), because of reduced effective evapotranspiration. There is evidence of high rainfall between 7.9 and 7.4 ka in Corchia Cave, Italy and Soreq Cave in Israel (Zanchetta et al. 2007) which supports this interpretation, even if the KTR-2 response was apparently more episodic. A dark layer in KTR-2 hand specimen at ~7.8 ka coincides with lateral crystal growth fabrics and a peak in $\delta^{13}\text{C}$. The crystal fabrics may indicate growth in a thin water film, but not in this case accompanied by either a marked hiatus or Cm fabrics; a constant drip rate is inferred. By 7.2 ka, both $\delta^{18}\text{O}$ and $\delta^{13}\text{C}$ show large positive excursions indicating the onset of renewed aridity followed by cessation of stalagmite growth perhaps indicating complete dryness in the epikarst.

The increased aridity, marked by increased $\delta^{13}\text{C}$ at 7.2 ka, corresponds with the end of S1 deposition (Fig. 13) at ~7.0 to 7.1 ka in the N Aegean, Ionian and Adriatic Seas (Kotthoff et al. 2008b; Emeis et al. 2000, Geraga et al. 2008; Rohling et al. 1997). Drying at this time is also manifest in reduced precipitation at the Alkyas Lagoon, Zakynthos (Avramidis et al. 2013) and in Lake Accesa, Italy (Peyron et al. 2011). This ‘end S1’ timing also broadly matches changes in hydrological conditions recorded in speleothems from Corchia Cave, Italy (Zanchetta et al. 2007), and Soreq Cave in Israel (Bar Matthews et al. 1999).

6.3. Alluvial fan record

The gravel-dominated parts of the sedimentary sequence were mostly active during episodes of high winter runoff, followed by inactivity during the dry summers, probably with extensive deciduous oak woodland on the upper fan and fan margins as indicated by palynological data from the offshore Corinthian Gulf (Collier et al. 2000).

The abundance of Fe oxides in the thin palaeosols (Fig. 11) reflects the ultrabasic substrate upon which they developed, rich in Fe-bearing olivine and orthopyroxene. These provide high pH soil microenvironments conducive to oxidative weathering, clay diagenesis and Fe^{3+} accumulation, probably from ferrihydrite precursors (see Schwertmann et al. 2004). The lack of horizonation implies these are entisols, i.e. weakly developed mineral soils with an ochric epipedon (Brady and Weil 2002). Comparison with active Fan D, 2 km to the E of

our study site (Collier et al., 1988), suggests they represent lower fan surfaces, largely devoid of vegetation, where exposure and oxidation of the clastic substrate led to limited silt and clay production. The similarity of silt layer spacings and erosion features above the most prominent 30 cm thick palaeosol at both locations allow correlation between the sea cliff and quarry sections (Fig. 10). If correctly correlated, the different ages determined for the same palaeosol require explanation. We suggest the palaeosol developed slowly, episodically and possibly diachronously over a long period of time (the ages allow ~9.5 to 8.3 ka) with millimetric differences in sample depth below top, having a profound effect on age. This suggests that the younger age in the quarry section (8.3-8.4 ka) marks the final phase, and culmination of pedogenesis.

The basal palaeosol in the sea cliff section, with an age ~9.3 ka, is separated from the overlying palaeosol by 'normal' alluviation, and the bracketing ages (despite possible inversion of <400 years) suggest almost instantaneous flood deposition of this unit. The ages are too young to register the Preboreal Oscillation but they broadly confirm that periodic pedogenesis was ongoing by ~9.5 ka following ~700 years of wet conditions as recorded in KTR-2 (Fig. 12). The 9.3 ka palaeosol age is within error of the ~9.2 ka climatic anomaly (Fleitmann et al., 2008) although this event has no signature in the KTR-2 record.

The KTR-2 record shows that drying had certainly re-established by 8.8 ka, and the 30 cm thick, light red entisol in the quarry section (Fig. 11) fixes culmination of this (probably prolonged) pedogenesis at 8.3 to 8.4 ka, within error of the 8.2 ka climatic event. KTR-2 $\delta^{13}\text{C}$ values between -5.5 and -6.0 ‰ at this time indicate dry conditions with entisol development recording pedogenesis following abandonment of this part of the active fan.

Fine-grained alluvial fan sedimentation had resumed ~7.8-7.9 ka in the seacliff section (Figs 9 and 10), coincident with indications of wetter climate (from $\delta^{13}\text{C}$ in KTR-2) particularly ~8.1-8.0 ka, but also episodically between 7.8 and 7.2 ka, the latter overlapping wetter climate indications ~7.5 ka in nearby lake Stymphalia (Heymann et al., 2103). Resumption of alluviation in the quarry section occurred later, the 8.3 to 8.4 ka age palaeosol not overwhelmed by 'normal' streamflow alluvium for a further ~3000 years, when aggradation allowed spillover onto the reactivated fan surface. A total of around 6 m accumulated over an unconstrained time to the present-day inactive fan surface (Fig. 10).

Lower down the fan, the youngest centimetric-scale upper palaeosol seen in the sea cliff developed around 5.0 ka, in response to a channel/lobe switch that subsequently reversed and

deposited the youngest prism of sediment on the easternmost flanks of the fan. This last depositional event was foreclosed as marine erosion began the slow retreat of the fan's eastern coastal cliff line promoting channel incision and abandonment of many of the lower fan lobes. The palaeosol age of 5.0 ka is too young for comparison with the KTR-2 record but consistent with aridity indicators ~5.0 ka in the Lake Stymphalia record (Heymann et al., 2013). In central Italy and the Levant, Zanchetta et al. (2014) detect a speleothem isotopic excursion argued to reflect relatively drier winters including a short sub-centennial period around 5.2 ka. In Lebanon, Cheng et al. (2015) detect strong Bond event aridity at 5.1 ka.

7. 8.2 ka regional climate effects

While the KTR-2 record contains petrographic and isotopic evidence of developing if episodic dryness between 8.8 and 8.2 ka, wetter conditions between 8.5 and 8.4 ka are also evident in both the isotopic and elemental proxies. Indications of more humid summers between 8.7 and 8.5 ka in nearby Lake Stymphalia (Heymann et al., 2013) might implicate a change in the timing of recharge, from winter to summer, around 8.5 ka. The combined information indicates that developing dryness approaching 8.2 ka was not as marked as it had been in the early Holocene, an interpretation corroborated by the moderate KTR-2 extension rates ($\sim 2.9 \text{ cm ka}^{-1}$; Fig. 4) approaching 8.2 ka, relative to the slower early Holocene rates ($\sim 1.1 \text{ cm ka}^{-1}$; Fig. 4). Moreover, between 8.5 and 8.4 ka, decrease in $\delta^{13}\text{C}$ could be indicating that above-cave vegetation growth was reinvigorated, perhaps by increased convective summer precipitation coinciding with the growing season.

The stalagmite data is thus consistent with Aegean hinterland vegetation records that indicate a fundamental change in hydrological conditions from wet to drier winters. Specifically, deciduous tree pollen percentage in Aegean marine cores declines from 8.4 ka with sharp reduction at 8.2 ka, especially noticeable in the reduced proportion of evergreen oaks (Fig. 13) that are sensitive to winter drought (Kotloff et al. 2008a, 2008b; Pross et al. 2009). Analogy with present day Mediterranean climate dynamics suggests this was caused by blocking of Atlantic fronts that intrude westward and trigger internal winter Mediterranean cyclogenesis (Meteorological Office 1962; Trigo et al. 2000, 2002). However, microfaunal and palynological data from both terrestrial northern Greece (Peyron et al. 2011) and the SE Aegean (Triantaphyllou et al. 2009) also indicate a parallel increase in summer precipitation. This may implicate an 8.2 ka-driven (cold N Atlantic) intensification of the Siberian high

pressure, blocking Atlantic fronts, a weakened summer monsoon (Wang et al., 2005; Cheng et al., 2009) and reduced subsidence over the eastern Mediterranean promoting vigorous summer cyclogenesis (cf. Trigo et al., 2002). Whatever the precise mechanism the precipitation regime of the eastern Mediterranean changed its pattern from winter frontal to summer convective over less than 1000 years.

If palaeosol development on Fan F was randomly distributed in time and space, then it is simply coincidence that the MRT age for the culmination of the thickest entisol aligns with climatic aridity at 8.2 ka. Alternatively, and perhaps more likely, the development of palaeosols was driven by climatic events. If this is accepted, there are two scenarios that may account for palaeosol development:

1. The whole of the eastern lower fan essentially dried up, the cessation of sedimentation allowing entisol development.
2. A change in precipitation regime from winter frontal to summer convective promoted 'flashier' summer rainfall regimes, perhaps with exceptional floods that caused rapid fan-channel incision. The incision isolated large areas of surface fan and the onset of prolonged pedogenesis there. Reduced rains from diminished winter cyclogenesis may have promoted winter drought, slowing cool season pedogenesis and reducing evergreen *Quercus* canopies further, enhancing summer runoff and sediment erosion.

Given that the KTR-2 record suggests episodic dryness and Aegean hinterland vegetation records suggest episodic convective summer rainfall in the period between 8.8 and 8.1 ka, we prefer scenario 2 as a likely driver for entisol development at 8.2 ka. Allocyclic channel incision on the lower fan is likely to have been caused mainly by flash flooding before the sea level highstand (~7 ka), whereas after the highstand, sea cliffing of the fan toe would have also contributed to incision. The main weakness of this interpretation is that so far, exposures in the lower fan have not been extensive enough to reveal the incised channel network required in this scenario.

8. Conclusions

We have outlined a case study from southern Greece, that for the first time, links regional Holocene palaeoclimate change from a montane speleothem record with the sedimentary response of a range front, semi-arid alluvial fan using dated sedimentary records.

1. Variations in $\delta^{13}\text{C}$ in a stalagmite from southern Greece best record the main elements of regional early Holocene palaeoclimate in southern Greece that are consistent with other regional proxies. The $\delta^{13}\text{C}$ values, reflecting soil carbon input to karst groundwater, indicate dry conditions before 10.3 ka, followed by a wetter interval starting around 10.3 ka, but interrupted by dryer conditions between 8.8 and 8.2 ka. Wetter conditions re-established after 8.1 ka to the end of the record. Of the three largest early Holocene cool and dry climatic anomalies only the 8.2 ka event has expression in the stalagmite stable isotope data.
2. While developing, if episodic, dryness is clearly evident in the stalagmite record between 8.8 and 8.2 ka, the markedly cool and dry conditions predicted for the N Hemisphere at 8.2 ka, are not particularly strongly developed, in common with a number of other stalagmite climate records from the wider Mediterranean regions.
3. Palaeosols on alluvial Fan F developed slowly, episodically and possibly diachronously over a long period of time (the calibrated radiocarbon ages allow ~9.5 to 8.3 ka). The thickest entisol, dated to 8.3-8.4 ka marks the culmination of pedogenesis within error of the 8.2 ka climatic event. We interpret this pedogenesis as a non-random, allocyclic response, driven by climatic events recorded in the stalagmite and other climatic proxies.
4. For the 8.2 ka event, temporary development of 'flashier' summer rainfall regime causing fan-channel incision is a plausible mechanism for allocyclic control on palaeosol development. Our attribution of the causes of incision remains speculative in the absence of better exposures; however, our approach outlines how radiocarbon chronology for alluvial fan palaeosols can be used for centennial-timeframe interpretation of alluvial fan response to climatic drivers.

ACKNOWLEDGEMENTS

Mr Giannopoulos, the owner of Limon Cave, kindly allowed us to sample in the cave and collected some of the drip water samples. Stephen Winser made helpful observations at Vamvakes and Schinos and shared geomorphological information on the fan catchments. Jenny Mason allowed us to use some of her unpublished thesis data. Alan Kendall gave sage advice on petrography and comments from Sophie Verheyden and Alex Brasier at various stages encouraged us to keep going. Anonymous journal reviewers also gave helpful advice. Graham Chilvers ran the LA-ICPMS and assisted with data reduction. EP acknowledges

receipt of a NERC studentship through grants NE/L50158X/1 and NE/K500896/1. Support for U/Th dating was through award IP-1410-1110 from the NERC Isotope Geosciences Facility. Radiocarbon dating was funded through the Syn-Rift Systems project funded by Research Council of Norway (Project number 255229/E30) and industry partners Aker BP, ConocoPhillips, Faroe Petroleum, Statoil, Tullow Oil and VNG Norge. We would like to dedicate this paper to the late Prof Keith Briffa, a fine UEA colleague and inspirational Holocene palaeoclimatologist.

Data Availability

Datasets related to this article can be found at [xxxx url], hosted at [xxxxx] ([Peckover et al., 2019]).

REFERENCES

- Alley, R.B., Mayewski, P.A., Sowers, T., Stuiver, M., Taylor, K.C. and Clark, P.U., 1997. Holocene climatic instability: a prominent, widespread event 8200 yr ago: *Geology*, 25, 483-486.
- Alley, R.B. and Ágústsdóttir, A.M., 2005. The 8K event: cause and consequences of a major Holocene abrupt climate change: *Quaternary Science Reviews*, 24, 1123-1149.
- Andersen, K.K., Azuma, N., Baronola, J.-M. et al. 2004. High-resolution record of Northern Hemisphere climate extending into the last interglacial period. *Nature*, 431, 147-151.
- Andersen, M. B., Stirling, C. H., Potter, E.-K., Halliday, A. N., Blake, S. G., Mcculloch, M. T., Ayling, B. F. and O'leary, M. 2008. High-precision U-series measurements of more than 500,000 year old fossil corals. *Earth and Planetary Science Letters*, 265, 229-245.
- Antinao, J.L., McDonald, E., Rhodes, E.J., Brown, N., Barrera, W., Gosse, J.C. and Zimmerman, S. 2016. Late Pleistocene-Holocene alluvial stratigraphy of southern Baja California, Mexico. *Quaternary Science Reviews*, 146, 161-181.
- Avramidis, P., Geraga, M., Lazarova, M. and Kontopoulos, N. 2013. Holocene record of environmental changes and palaeoclimatic implications in Alykes Lagoon, Zakynthos Island, western Greece, Mediterranean Sea. *Quaternary International*, 293, 184-195. doi: 10.1016/j.quaint.2012.04.026.
- Barber, D.C., Dyke, A., Hillaire-Marcel, C., Jennings, A.E., Andrews, J.T., Kerwin, M.W., Bilodeau, G., McNeely, R., Southon, J., Morehead, M.D. and Gagnon, J.-M. 1999. Forcing of

the cold event of 8,200 years ago by catastrophic drainage of Laurentide lakes. *Nature*, 400, 344-348.

Bard, E., Delaygue, G., Rostek, F., Antonioli, F., Silenzi, S., and Schrag, D.M. 2002. Hydrological conditions over the western Mediterranean basin during the deposition of the cold Sapropel 6 (ca. 175 kyr BP). *Earth and Planetary Science Letters*, 202, 481-494.

Bar-Matthews, M., Ayalon, A., Gilmour, M., Matthews, A. and Hawkesworth, C. J. 2003. Sea-land oxygen isotopic relationships from planktonic foraminifera and speleothems in the Eastern Mediterranean region and their implication for paleorainfall during interglacial intervals. *Geochimica et Cosmochimica Acta*, 67, 3181-3199. doi: 10.1016/S0016-7037(02)01031-1.

Bar-Matthews, M., Ayalon, A., Kaufman, A. and Wasserburg, G. J. 1999. The Eastern Mediterranean paleoclimate as a reflection of regional events: Soreq cave, Israel. *Earth and Planetary Science Letters*, 166, 85-95. doi: 10.1016/S0012-821X(98)00275-1.

Brady, N.C. and Weil, R.R. (2002) Soil classification. Chapter 3, pp. 75-120, *The Nature and Properties of Soils*, 13th Ed., Prentice Hall, New Jersey.

Brasier, A.T., Andrews, J.E., Marca-Bell, A., and Dennis, P.F. 2010. Depositional continuity of seasonally laminated tufas: implications for $\delta^{18}\text{O}$ based palaeotemperatures. *Global and Planetary Change*, 71, 160-167. doi:10.1016/j.gloplacha.2009.03.022

Boch, R., Spötl, C. and Frisia, S. 2011. Origin and palaeoenvironmental significance of lamination in stalagmites from Katerloch Cave, Austria. *Sedimentology*, 58, 508-531. doi.org/10.1111/j.1365-3091.2010.01173.x

Bordon, A., Peyron, O., Lézine, A., Brewer, S. and Fouache, E. 2009. Pollen-inferred Late-Glacial and Holocene climate in southern Balkans (Lake Maliq). *Quaternary International*, 200, 19-30. doi: 10.1016/j.quaint.2008.05.014.

Bowen G. J. and Revenaugh J. 2003. Interpolating the isotopic composition of modern meteoric precipitation. *Water Resources Research* 39, 1299, doi:10.129/2003WR002086.

Bowen G. J. and Wilkinson B. 2002. Spatial distribution of $\delta^{18}\text{O}$ in meteoric precipitation. *Geology* 30, 315-318.

Cheng, H., Edwards, R. L., Hoff, J., Gallup, C., D. Richards, D. A. and Asmerom, Y. 2013. The half-lives of uranium-234 and thorium-230. *Chemical Geology*, 169, 17-33.

Cheng, H., Fleitmann, D., Edwards, R.L., Wang, X., Cruz, F.W., Auler, A.S., Mangini, A., Wang, Y, Kong, X., Burns, S.J, and Matter, A. 2009. Timing and structure of the 8.2 kyr B.P. event inferred from $\delta^{18}\text{O}$ records of stalagmites from China, Oman, and Brazil. *Geology*, 37, 1007-1010.

Cheng, H., Sinha, A., Verheyden, S., Nader, F. H., Li, X. L., Zhang, P. Z., Yin, J. J., Yi, L., Peng, Y. B., Rao, Z. G., Ning, Y. F., and Edwards, R. L. 2015. The climatic variability in northern Levant over the past 20 000 years. *Geophysical Research Letters*, 42, 8641-8650.

Cheng, H., Zhang, P. Z., Spötl, C., Edwards, R. L., Cai, Y.J., Zhang, D. Z., Sang, W.C., Tan, M. and An, Z.S. 2012. The climatic cyclicity in semiarid-arid central Asia over the past 500,000 years. *Geophysical Research Letters*, 39, L01705, doi.org/10.1029/2011GL050202

Clarke, G.K.C., Leverington, D.W., Teller, J.T., and Dyke, A.S., 2004. Paleohydraulics of the last outburst flood from glacial Lake Agassiz and the 8200 BP cold event. *Quaternary Science Reviews*, 23, 389-407.

Collier, R.E.L., Leeder, M.R., Trout, M., Ferentinos, G., Lyberis, E. and Papatheodorou, G. 2000. High sediment yields and cool, wet winters: Test of last glacial paleoclimates in the northern Mediterranean. *Geology*, 28, 999-1002.

Collier, R.E.L., Pantosti, D., D'Addezio, G., De Martini, P.M., Masana, E., and Sakellariou, D. 1998. Paleoseismicity of the 1981 Corinth earthquake fault: Seismic contribution to extensional strain in central Greece and implications for seismic hazard. *Journal of Geophysical Research*, 103, 30,001–30,019.

Craig, H. 1961. Isotopic variations in meteoric waters. *Science*, 133, 1833-1834.

Daëron M., Drysdale, R.M., Peral, M., Huyghe, D., Blamart, D., Coplen, T.B., Lartaud, F., Zanchetta, G. 2019. Most Earth-surface calcites precipitate out of isotopic equilibrium. *Nature Communications* 10:429, <https://doi.org/10.1038/s41467-019-08336-5>, (7 pp.)

Dotsika, E., Lykoudis, S. and Poutoukis, D. 2010. Spatial distribution of isotopic composition of precipitation and spring water in Greece. *Global and Planetary Change*, 71, 141-149.

Drysdale, R., Hellstrom, J., Zanchetta, G., Fallick, A., Sánchez Goñi, M., Couchoud, I., McDonald, J., Mass, R., Lohmann, G. and Isola, I. 2009. Evidence for obliquity forcing of glacial termination II. *Science*, 325, 1527–1531. doi: 10.1126/science.1170371.

Ellison, C., Chapman, M., and Hall, I. (2006) Surface and deep ocean interactions during the cold climate event 8200 years ago. *Science*, 312, 1929-1932.

Emeis, K.-C., Struck, U., Schulz, H.-M., Rosenberg, R., Bernasconi, S., Erlenkeuser, H., Sakamoto, T. and Martinez-Ruiz, F. 2000. Temperature and salinity variations of Mediterranean Sea surface waters over the last 16, 000 years from records of planktonic stable oxygen isotopes and alkenone unsaturation ratios. *Palaeogeography, Palaeoclimatology Palaeoecology*, 158, 259–280. doi: 10.1016/S0031-0182(00)00053-5.

Fairchild, I.J. and Baker, A. 2012. *Speleothem Science: from Process to Past Environments*. John Wiley and Sons, Ltd, Chichester, UK. <http://dx.doi.org/10.1002/9781444361094>.

Fairchild, I.J., Borsato, A., Tooth, A.F., Frisia, S., Hawkesworth, C.J., Huang, Y., McDermott,

F. and Spiro, B., 2000. Controls on trace element (Sr–Mg) composition of carbonate cave waters: implications for speleothem climatic records. *Chemical Geology*, **166**, 255–269.

Finné, M., Bar-Matthews, M., Holmgren, K., Sundqvist, H.S., Liakopoulos, I., and Zhang, Q. 2014. Speleothem evidence for late Holocene climate variability and floods in Southern Greece. *Quaternary Research*. 81, 213-227. <http://dx.doi.org/10.1016/j.yqres.2013.12.009>.

Fisher, T.G., Smith, D.G., and Andrews, J.T., 2002. Preboreal oscillation caused by a glacial Lake Agassiz flood: *Quaternary Science Reviews*, 21, 873–878.

Fleitmann, D., Mudelsee, M., Burns, S.J., Bradley, R.S., Kramers, J. and Matter, A. 2008 Evidence for a widespread climatic anomaly at around 9.2 ka before present. *Paleoceanography*, 23, PA 1102. doi:10.1029/2007PA001519.

Flocas, A. A. and Giles, B. D. 1991. Distribution and intensity of frontal rainfall over Greece. *International Journal of Climatology*, 11, 429–442. doi:10.1002/joc.3370110407.

Francke, A., Wagner, B., Leng, M. J. and Rethemeyer, J. 2013. A Late Glacial to Holocene record of environmental change from Lake Dojran (Macedonia, Greece). *Climate of the Past Discussions*, 8, 5743–5785. doi: 10.5194/cpd-8-5743-2012.

Frisia, S. 2015. Microstratigraphic logging of calcite fabrics in speleothems as tool for palaeoclimate studies. *International Journal of Speleology*, 44, 1-16. doi.org/10.5038/1827-806X.44.1.1

Frisia, S. and Borsato, A. 2010. Carbonates in Continental Settings: Facies, Environments, and Processes. Chapter 6 Karst.,” *Developments in Sedimentology*. Elsevier (*Developments in Sedimentology*), 61, pp. 269–318. doi: 10.1016/S0070-4571(09)06106-8.

Frisia, S., Borsato, A., Fairchild, I. J. and Dermott, F. M. C. 2000. Calcite fabrics, growth mechanisms, and environments of formation in speleothems from the Italian Alps and

south western Ireland. *Journal of Sedimentary Research*, 70, 1183–1196. doi: 10.1306/022900701183.

Frumkin, A., Schwarcz, H. P. and Ford, D. C. 1994. Evidence for isotopic equilibrium in stalagmites from caves in a dry region: Jerusalem, Israel. *Israel Journal of Earth Sciences* 43, 221–230.

Garcia, A.F. and Stokes, M. 2006. Late Pleistocene highstand and recession of a small, high-altitude pluvial lake, Jakes Valley, central Great Basin, USA. *Quaternary Research*, 65, 179–186.

Gat, J.R. and Carmi, I., 1970. Evolution of the isotopic composition of atmospheric waters in the Mediterranean Sea area. *J. Geophys. Res.* 75, 3039–3048.

Geraga, M., Mylona, G., Tsaila-Monopolis, S., Papatheodorou, G. and Ferentinos, G. 2008. Northeastern Ionian Sea: Palaeoceanographic variability over the last 22 ka. *Journal of Marine Systems*, 74, 623–638. doi: 10.1016/j.jmarsys.2008.05.019.

Gogou, A., Bouloubassi, I., Lykousis, V. and Arnaboldi, M. 2007. Organic geochemical evidence of Late Glacial – Holocene climate instability in the North Aegean Sea. *Palaeogeography, Palaeoclimatology, Palaeoecology*, 256, 1–20. doi: 10.1016/j.palaeo.2007.08.002.

Grant, K.M., Grimm, R., Mikolajewicz, U., Marino, G., Ziegler, M. and Rohling, E.J. 2016. The timing of Mediterranean sapropel deposition relative to insolation, sea-level and African monsoon changes. *Quaternary Science Reviews*, 140, 125–141. doi.org/10.1016/j.quascirev.2016.03.026

Harvey, A.M., Wingland, P.E. and Wells, S.G. 1999. Response of alluvial fan systems to the late Pleistocene to Holocene climatic transition: contrasts between the margins of pluvial Lakes Lahontan and Mojave, Nevada and California, USA. *Catena*, 36, 255–281.

Heymann, C., Nelle, O., Dörfler, W., Zagana, H., Nowaczyk, N., Xue, J. and Unkel, I. 2013. Late Glacial to mid-Holocene palaeoclimate development of Southern Greece inferred from the sediment sequence of Lake Stymphalia (NE-Peloponnese). *Quaternary International*, 302, 42–60 doi: 10.1016/j.quaint.2013.02.014.

Hiess, J., Condon, D. J., McLean, N., and Noble, S. R. 2012. $^{238}\text{U}/^{235}\text{U}$ systematics in terrestrial uranium-bearing minerals: *Science*, 335, 1610–1614.

Iliopoulou-Georgudaki, J. and Economidou, E. 1991. Ecological study and management of the cave “Limnon” Peloponnese, Greece. *Mémoires de Biospéologie*, XVIII, 93–97.

Jackson, J.A., Gagnepain, J., Houseman, G., King, G., Papadimitriou, P., Soufleris, C., and Virieux, J. 1982. Seismicity, normal faulting, and the geomorphological development of the

Gulf of Corinth (Greece): The Corinth earthquakes of February and March 1981: *Earth and Planetary Science Letters*, 57, 377–397.

Kambezidis, H. D., Larissi, I. K., Nastos, P. T. and Paliatsos, A. G. 2010. Spatial variability and trends of the rain intensity over Greece. *Advances in Geosciences*, 26, 65–69. doi: 10.5194/adgeo-26-65-2010.

Kendall, A.C. and Broughton, P.L., 1978. Origin of fabric in speleothems of columnar calcite crystals. *Journal of Sedimentary Petrology* 48, 550-552.

Kim, S. T., and O'Neil, J. R. 1997. Equilibrium and nonequilibrium oxygen isotope effects in synthetic carbonates: *Geochimica et Cosmochimica Acta*, 61, 3461-3475.

Kottoff, U., Pross, J., Müller, U.C., Peyron, O., Schmiedl, G., Schulz, H. and Bordon, A. 2008a. Climate dynamics in the borderlands of the Aegean Sea during formation of Sapropel S1 deduced from a marine pollen record. *Quaternary Science Reviews*, 27, 832-845.

Kottoff, U., Müller, U.C., Pross, J., Schmiedl, G., Lawson, I.T., van der Schootbrugge, B., and Schulz, H. 2008b. Lateglacial and Holocene vegetation dynamics in the Aegean region: an integrated view based on pollen data from marine and terrestrial archives. *The Holocene*, 18, 1019-1032.

Leeder, M.R., Seger, M.J. and Stark C.P. 1991. Sedimentation and tectonic geomorphology adjacent to major active and inactive normal faults, southern Greece, *J. Geol. Soc. London*. 148, 331-343.

Leeder, M.R., Collier, R.E.L., Aziz, L.H.A., Trout, M., Ferentinos, G., Papatheodorou, G. and Lyberis, E. 2002. Tectono-sedimentary processes along an active marine/lacustrine half-graben margin: Alkyonides Gulf, E. Gulf of Corinth, Greece. *Basin Research*, 14, 25-41, <http://doi.org/10.1046/j.1365-2117.2002.00164.x>

Leeder, M.R., Harris, T. and Kirkby, M.J. 1998. Sediment supply and climate change: implications for basin stratigraphy *Basin Research*, 10, 7-18.

Marino, G., Rohling, E. J., Sangiorgi, F., Hayes, A., Casford, J. L., Lotter, A. F., Kucera, M. and Brinkhuis, H. 2009. Early and middle Holocene in the Aegean Sea: interplay between high and low latitude climate variability. *Quaternary Science Reviews*, 28, 3246–3262. doi: 10.1016/j.quascirev.2009.08.011.

Mason, J. E. 2009. Palaeoclimatic Records from Speleothems in the Eastern Mediterranean. PhD thesis, University of East Anglia, Norwich UK, 234pp.

Mechernich, S., Schneiderwind, S., Mason, J., Papanikolaou, I. D., Deligiannakis, G., Pallikarakis, A., Binnie, S. A., Dunai, T.J. and Reicherter, K. 2018. The seismic history of the

Pisia fault (eastern Corinth rift, Greece) from fault plane weathering features and cosmogenic ^{36}Cl dating. *Journal of Geophysical Research: Solid Earth*, 123, 4266–4284. <https://doi.org/10.1029/2017JB014600>.

Mercone, D., Thomson, J., Abu-Zied, R. H., Croudace, I. W. and Rohling, E. J. 2001. High resolution geochemical and micropalaeontological profiling of the most recent eastern Mediterranean sapropel. *Marine Geology*, 177, 25–44.

Meteorological Office, 1962. *Weather in the Mediterranean* (2nd edn), vol. 1. Air Ministry, British Meteorological Office. HMSO: London.

Meyers, P. A., and Arnaboldi, M. 2008. Paleooceanographic implications of nitrogen and organic carbon isotopic excursions in mid-Pleistocene sapropels from the Tyrrhenian and Levantine Basins, Mediterranean Sea. *Palaeogeography, Palaeoclimatology, Palaeoecology*. 266, 112-118. doi.org/10.1016/j.palaeo.2008.03.018.

Peyron, O., Goring, S., Dormoy, I., Kotthoff, U., Pross, J., de Beaulieu, J.-L., Drescher-Schneider, R., Vanni re, B. and Magny, M. 2011. Holocene seasonality changes in the Central Mediterranean region reconstructed from the pollen sequences of Lake Accessa (Italy) and Tenaghi Philippon (Greece). *The Holocene*, 21, 131-146.

Pope, R. J., Hughes, P.D. and Skourtsos, E. 2017 Glacial history of Mt Chelmos, Peloponnesus, Greece. *Geological Society, London, Special Publication*, 433, 211-236. doi.org/10.1144/SP433.11

Pross, J., Kotthoff, U., M ller, U.C., Peyron, O., Dormoy, I., Schmiedl, G., Kalaitzidis, S., and Smith A.M. 2009. Massive perturbation in terrestrial ecosystems of the Eastern Mediterranean region associated with the 8.2 kyr B.P. climatic event. *Geology*, 37, 887-890.

Reheis, M.C., Slate, J.L., Throckmorton, C.K., McGeehn, J.P. Sarna-Woicicki, A.M. and Dangler, L. 1996. Late Quaternary sedimentation on the Leidy Creek fan, Nevada-California: geomorphic response to climate change. *Basin Research*, 8, 279-299.

Reimer, P.J., Bard, E., Bayliss, A., Beck, J.W., Blackwell, P.G., Bronk Ramsey, C., Buck, C.E., Cheng, H., Edwards, R.L., Friedrich, M., Grootes, P.M., Guilderson, T.P., Haflidason, H., Hajdas, I., Hatt , C., Heaton, T.J., Hoffmann, D.L., Hogg, A.G., Hughen, K.A., Kaiser, K.F., Kromer, B., Manning, S.W., Niu, M., Reimer, R.W., Richards, D.A., Scott, E.M., Southon, J.R., Staff, R.A., Turney, C.S.M. and van der Plicht, J. 2013. IntCal13 and Marine13 radiocarbon age calibration curves 0–50,000 years cal BP. *Radiocarbon* 55, 1869–1887.

Renssen, H., Goosse, H. and Fichefet, T. 2002, Modeling the effect of freshwater pulses on early Holocene climate: The influence of high-frequency variability: *Palaeoceanography*, 17, 1-10.

Ritter, J.B., Miller, J.R., Enzel, Y. and Wells, S.G. 1995. Reconciling the roles of tectonism and climate in Quaternary fan evolution. *Geology*, 23, 245-248.

Roberts, M.S., Smart, P.L., Hawkesworth, C.J., Perkins, W.T. and Pearce, N.J.G., 1999. Trace element variations in coeval Holocene speleothems from GB Cave, southwest England. *The Holocene*, 9, 707–713.

Rohling, E. J., Jorissen, F. J. and De Stigter, H. C. 1997. 200 Year interruption of Holocene sapropel formation in the Adriatic Sea. *Journal of Micropalaeontology*, 16, 97–108. doi: 10.1144/jm.16.2.97.

Rohling, E.J., Marino, G., Grant, K.M. 2015. Mediterranean climate and oceanography, and the periodic development of anoxic events (sapropels). *Earth-Science Reviews*, 143, 62-97. doi.org/ 10.1016/j.earscirev.2015.01.008.

Rohling, E.J., Mayewski, P.A., Abu-Zied, R.H., Casford, J.S.L., Hayes, A. 2002. Holocene atmosphere-ocean interactions: records from Greenland and the Aegean Sea. *Climate Dynamics*, 18, 587-593.

Rohling, E.J. and Pälike, H. 2005. Centennial-scale climate cooling with a sudden cold event around 8,200 years ago. *Nature*, 434, 975-979.

Royle, S., Andrews, J.E., Turner, J. and Kružić, P. 2015. Environmental and diagenetic records from trace elements in the Mediterranean coral *Cladocora caespitosa*. *Palaeogeography, Palaeoclimatology, Palaeoecology*, 440, 734-749. 10.1016/j.palaeo.2015.10.010

Scholz, D., and Hoffmann, D. L. 2011, StalAge - An algorithm designed for construction of speleothem age models. *Quaternary Geochronology*, 6, 369-382.

Schwertmann, U., Stanjek, H., and Becher, H.H. 2004, Long-term in vitro transformation of 2-line ferrihydrite to goethite/haematite at 4, 10, 15 and 25 degrees C. *Clay Minerals* 39, 433-438.

Spurk, M., Leuschner, H-H., Baillie, M.G.L., Briffa, K.R., and Friedrich M. 2002. Depositional frequency of German subfossil oaks: climatically and non-climatically induced fluctuations in the Holocene. *The Holocene*, 12, 707-715.

Stokes, M., Nash, D.J. and Harvey, A.M. 2007. Calcrete ‘fossilisation’ of alluvial fans in SE Spain: The roles of groundwater, pedogenic processes and fan dynamics in calcrete development. *Geomorphology*, 85, 63-84. doi:10.1016/j.geomorph.2006.03.020.

Talbot, M.R. and Williams, M.A.S. 1979. Cyclic alluvial fan sedimentation on the flanks of fixed dunes, Janjari, Central Niger. *Catena*, 6, 43-62.

Taylor, S.R. and McLennan, S.M. 1995. The geochemical evolution of the continental crust. *Reviews of Geophysics*, 33, 241-265.

Teller, J. T. and Leverington, D. W. 2004. Glacial Lake Agassiz: A 5000 yr history of change and its relationship to the $\delta^{18}\text{O}$ record of Greenland, *Geological Society America Bulletin*, 116, 729-742.

Thomas, E. R., Wolff, E.W., Mulvaney, R., Steffensen, J.P., Johnsen, S.J., Arrowsmith, C., White, J W. C. Vaughn, B. and Popp, T. 2007. The 8.2 ka event from Greenland ice cores. *Quaternary Science Reviews*, 26, 70-81. doi: <https://doi.org/10.1016/j.quascirev.2006.07.017>.

Tinner, W. and Lotter, A.F. 2001. Central European vegetation response to abrupt climate change at 8.2 ka. *Geology*, 29, 551-554.

Tremaine D. M. and Froelich P. N. 2013. Speleothem trace element signatures: a hydrological geochemical study of modern cave dripwaters and farmed calcite. *Geochimica, Cosmochimica Acta*, 121, 522-545. <http://dx.doi.org/10.1016/j.gca.2013.07.026>.

Tremaine, D. M., Froelich, P. N. and Wang, Y, 2011. Speleothem calcite farmed *in situ*: Modern calibration of $\delta^{18}\text{O}$ and $\delta^{13}\text{C}$ palaeoclimate proxies in a continuously-monitored natural cave system. *Geochimica et Cosmochimica Acta*, 75, 4929-4950. doi: 10.1016/j.gca.2011.06.005.

Triantaphyllou, M.V., Ziveri, P., Gogou, A., Marino, G., Lykousis, V., Bouloubassi, I., Emeis, K.-C., Kouli, K., Dimiza, M., Rosell-Melé, A., Papanikolaou, M., Katsouras, G. and Numez, N. 2009. Late Glacial-Holocene climate variability at the south-eastern margin of the Aegean Sea. *Marine Geology*, 266, 182-197.

Triantaphyllou, M. V, Gogou, A., Dimiza, M. D., Kostopoulou, S., Parinos, C., Roussakis, G., Geraga, M., Bouloubassi, I., Fleitmann, D., Zervakis, V., Velaoras, D., Diamantopoulou, A., Sampatakaki, A. and Lykousis, V. 2016. Holocene Climatic Optimum centennial-scale paleoceanography in the NE Aegean (Mediterranean Sea). *Geo-Marine Letters*, 36, 51-66. doi: 10.1007/s00367-015-0426-2.

Trigo, I.F., Davies, T.D. and Bigg, G.R. 2000, Decline in Mediterranean rainfall caused by weakening of Mediterranean cyclones. *Geophysical Research Letters*, 27, 2913-2916.

Trigo, I.F., Bigg, G.R. and Davies, T.D., 2002. Climatology of cyclogenesis mechanisms in the Mediterranean. *Monthly Weather Review*, 130, 549-569.

Verheyden, S., Nader, F. H., Cheng, H. J., Edwards, L. R. and Swennen, R. 2008. Paleoclimate reconstruction in the Levant region from the geochemistry of a Holocene stalagmite from the Jeita cave, Lebanon. *Quaternary Research*, 70, 368–381. doi: 10.1016/j.yqres.2008.05.004.

Vellinga, M., and Wood, R.A., 2002, Global climatic impacts of a collapse of the Atlantic thermohaline circulation. *Climate Change*, 54, 251–267.

Ventra, D. and Nichols, G.J. 2014. Autogenic dynamics of alluvial fans in endorheic basins: outcrop examples and stratigraphic significance. *Sedimentology*, 61, 767–791.

Vinther, B. M., Clausen, H. B. Johnsen, S. J., Rasmussen, S. O., Andersen, K. K., Buchardt, S. L., Dahl-Jensen, D., Seierstad, I. K., Siggaard-Andersen, M.-L., Steffensen, J. P., Svensson, A., Olsen, J. and Heinemeier, J. 2006. A synchronized dating of three Greenland ice cores throughout the Holocene. *Journal of Geophysical Research*, 111, D13102, doi:10.1029/2005JD006921.

Wang, Y.J., Cheng, H., Edwards, R.L., He, Y.Q., Kong, X.G., An, Z.S., Wu, J.Y., Kelly, M.J., Dykoski, C.A., Li, X.D., 2005. The Holocene Asian monsoon: links to solar changes and North Atlantic climate. *Science*, 308, 854–857.

Weiberg, E., Unkel, I., Kouli, K., Holmgren, K., Avramidis, P., Bonnier, A., Dibble, F., Finné, M., Izdebski, A., Katrantsiotis, C., Stocker, S.R., Andwinge, A., Baika, K., Boyd, M., Heymann, C. 2016. The socio-environmental history of the Peloponnese during the Holocene: Towards an integrated understanding of the past. *Quaternary Science Reviews*, 136 40–65. dx.doi.org/10.1016/j.quascirev.2015.10.042

Zanchetta, G. Bar-Matthews, M., Drysdale, R. N., Lionello, P., Ayalon, A., Hellstrom, J. C., Isola, I and Regattieri, E. 2014. Coeval dry events in the central and eastern Mediterranean basin at 5.2 and 5.6 ka recorded in Corchia (Italy) and Soreq caves (Israel) speleothems. *Global and Planetary Change*, 22, 130–139.

Zanchetta, G., Drysdale, R. N., Hellstrom, J. C., Fallick, A. E., Isola, I., Gagan, M. K. and Pareschi, M.T. 2007. Enhanced rainfall in the Western Mediterranean during deposition of sapropel S1: stalagmite evidence from Corchia cave (Central Italy). *Quaternary Science Reviews*, 26, 279–286. doi: 10.1016/j.quascirev.2006.12.003.

Figure captions

Fig. 1. Main panel shows location of the Schinos Bajada, Limnon Cave and Lake Stymphalia in the North Peloponnese and Corinth isthmus area of Greece. Insets show wider national and regional context where A – Athens; P – Patras; TP - Tenaghi Phillipon.

Fig. 2. Axial slab of twin stalagmite KTR-2 showing growth axes (blue dashed lines). All samples were taken from the left stalagmite and U/Th sample positions (red circles are accompanied by the dates. StalAge excluded sample KTR-2 6 from the age model (see text). Green dashed line indicates the base of Holocene calcite at 127 mm. Inset shows a cave plan of the first 600 m of the cave with stalagmite sample positions. All cave water samples were collected between these positions.

Fig. 3. Panoramic view and interpretive sketch over Schinos Bay looking south from 50 m above sea level into the footwall scarps and bajada (skyline is c. 850 m above m.s.l.) along the overlap zone between the Pisia (upper scarp) and Schinos (lower scarp) active normal faults (for general location see Fig. 1). The large sea-cliffed ('toecut') coalesced alluvial fan is Fan 'F' (left side) and 'G' (right side) of Leeder et al. (2002), fed by currently inactive catchments that drain Mesozoic limestone and serpentinite hinterlands.

Fig. 4. U-Th age-depth model derived by StalAge for the Holocene section of the KTR-2 (data in Table 2) excluding KTR2-6 (see text). Upper (blue) and lower (red) lines represent 2 s.d. errors. There is only one likely minor hiatus (at 96 mm), indicating largely continuous extension.

Fig. 5. Thin section photomicrographs of KTR-2 fabrics with 500 μm scale bar. a) typical columnar open (Co) calcite, b) columnar microcrystalline (Cm) calcite; c) horizontal growth of Co calcite from left flank at 31 mm (~ 7.8 ka); d) abrupt transition (arrow) between Cm and Co calcites defined by a detritus-rich layer at 96 mm (~ 9.4 ka).

Fig. 6. Axial low resolution $\delta^{18}\text{O}$ (panel a, red) and $\delta^{13}\text{C}$ (panel b, blue) data plotted on the StalAge timescale (Fig. 4).

Fig. 7. Axial high resolution $\delta^{18}\text{O}$ (panel a, red) and $\delta^{13}\text{C}$ (panel b, blue) micro-milled data plotted on the StalAge timescale between 8.6 and 7.9 ka.

Fig. 8. Variation in high-resolution $\delta^{18}\text{O}$ (red) and Mg/Ca (green; upper panel) and Mg/Sr (grey; lower panel) showing some similarity in profile shape. The age model is constrained by three U/Th ages shown as black dots with error bars above the plot. Note that the trace element axes are inverted to facilitate direct comparison to the negative upward $\delta^{18}\text{O}$ scale.

Fig. 9. Palaeosols in the modern seacliff, with arrows showing position of radiocarbon samples. a) Upper part of a 30 cm thick light red entisol (~ 9.5 - 9.7 ka) sharply overlain by a

silty layer (~7.8-7.9 ka). The overlying 60 cm of open framework streamflow gravels are topped by a thin, discontinuous entisol overlain by another silty layer. b) Showing lateral continuity and sharp upper surface of the 30 cm thick entisol, also erosional gutters cutting through the upper silt layer and discontinuous entisol.

Fig. 10. Stratigraphic logs for Fan F (location on Fig. 3) showing stream flow gravel units, silty layers, erosion surfaces and palaeosol horizons with calibrated radiocarbon date ranges (Table 3). Time marker for 8.2 ka shows temporal correlation. Between ~9.5 ka and 8.0 ka, palaeosol (orange shade) development was ongoing, possibly intensifying from NW to SE with time. Palaeosols are probably compound with numerous non-deposition time breaks. The streamflow gravel lobe above the 5.0 ka palaeosol in the sea cliff section is probably thickening to the SE. Apparent dip on the 5.0 ka palaeosol ~9° E but its exact relationship with the post 5.0 ka lobe in the quarry section is not exposed.

Fig. 11. a) Panorama of the c. 200 m lateral extent of prominent light red entisol in roadside quarry to the SE of the cliffed lateral margin to Fan F (Fig. 3). b) Close-up of the main entisol with the shallow-scoured base to the angular fan gravels that contain light-grey fine silt-with-granules units 10 cm or so above the underlying entisol. The entisol gave an 8.3 to 8.4 ka age, while the base of the light grey gravel unit above the entisol gave an age of 4.9 to 5.3 ka. The junction between entisol and gravel represents a depositional hiatus of some 3000 years.

Fig. 12. Low resolution KTR-2 stable isotope data ($\delta^{13}\text{C}$ blue, $\delta^{18}\text{O}$ red) related to regional and global palaeoclimate events. Horizontal green bar indicates duration of S1 in the Aegean. Vertical yellow bars help correlate events, bar width representing minimum error envelope of ± 60 years (from U-series dates). Onset of a warm and wet (climate optimum) conditions in KTR-2 ~10.3 ka (vertical yellow bar), marked by rapidly declining $\delta^{13}\text{C}$, coincident with a cold phase (%cold water cyanobacterium *S. elongatus*; Marino et al. 2009; light blue record) in otherwise warming SST trend in Aegean. Wetter conditions in Lake Stymphalia (Heymann et al., 2013; purple dataset) also start at this time. Between 8.8-8.2 ka $\delta^{13}\text{C}$ indicates a period of dryness. Both KTR-2 isotopes are relatively high between 8.1 and 8.2 ka (see Figs 7a and 13 for high resolution data), coincident with peak abundance (cool) of *S. elongatus* (Marino et al. 2009) and within error of the 8.2 ka cold event in NGRIP (grey record) (Andersen et al. 2004) and Lake Maliq (green record, Bordon et al. 2009). Warmer and wetter conditions in KTR-2 re-established after 8.2 ka.

Fig. 13. High-resolution stable isotope data (micro-milled samples) for the period around 8.2 ka in context with global and regional observations. Dryness indicators in KTR-2 (mainly in $\delta^{13}\text{C}$ blue but also in $\delta^{18}\text{O}$ in red) combine between 8.2 and 8.1 ka indicated by the vertical yellow bar. The bar width is a minimum error envelope (from U-series dates) of ± 60 years. This dry period is within error of the latter part of the NGRIP 8.2 ka cold event (dataset from Andersen et al. 2004). Regional dryness at this time is indicated by rapid declines in Tenaghi Philippon total tree and shrub pollen percentage from 8.4 ka (blue dataset; Peyron et al., 2011) as are the proportion of evergreen oaks (orange dataset). Cooling NE Aegean (Marino et al. 2009; green dataset) winter SSTs between 8.2 and 8.0 ka are indicated by higher percentages of *S. elongatus* a cold water cyanobacterium (Rohling et al. 2002). The KTR-2 dry phase also corresponds broadly to the timing of S1 disruption in the coastal Aegean Sea (purple bar; Kotthoff et al. 2008b).

Table 1. Stable isotope composition of active calcites in Limnon Cave forming within 150 m of KTR-2. The temperatures are calculated from the calcite $\delta^{18}\text{O}$ values using the equilibrium equation of Tremaine et al. (2011) and, for comparison, that of Kim and O'Neil (1997). A mean cave water $\delta^{18}\text{O}$ of -7.5‰ VSMOW was used for all temperature calculations (see text). Values in bold calculated from Tremaine et al. (2011) overlap with measured winter cave temperatures. Walkway deposit value is probably disequilibrium (see Supplementary information) and is excluded from means.

Table 2. U-series data for stalagmite KTR2. Sample weights ~ 150 mg. Note age inversion in samples KTR2-5 and KTR2-6 (shaded), the latter was omitted from the age model (see text). All errors are 2σ . Isotope ratios in brackets denote activity ratios and were calculated using the decay constants of Cheng et al. (2013). Numbers in parenthesis are ratio errors for the last reported digits. Ages BP refer to 2016, the date of analysis. Ages were corrected assuming a contaminant of bulk earth composition with a Th/U weight ratio = 3.8 (Taylor and McLennan, 1995), assumed error of 50% and ^{238}U , ^{234}U and ^{230}Th in secular equilibrium.

Table 3. AMS ^{14}C dates of palaeosol and associated fine-grained matrix sediments from Schinos Fan F. All dates by *Beta Analytic Inc.* calibrated using IntCal13. Age for sample MRL109914-5 originally published in Leeder et al. (2002)

Table 1

	$\delta^{18}\text{O}$ (‰ VPDB)	$\delta^{13}\text{C}$ (‰ VPDB)	τ °C (Kim & O'Neil 1997)	τ °C (Tremaine et al., 2011)
Active straw stalactite	-6.3	-8.7	9.4	13.1
Top of active stalagmite KTR-1	-6.2	-8.5	8.9	12.6
Active stalactite drape	-6.2	-7.9	8.9	12.6
Calcite deposit on metal walkway	-6.8	-11.6	11.6	15.7
Mean	-6.2	-8.3		

Table 2

Sample Number	Depth from top (mm)	^{238}U (ppm)	^{232}Th (ppb)	$(^{234}\text{U}/^{238}\text{U})$	$(^{230}\text{Th}/^{238}\text{U})$	$(^{230}\text{Th}/^{232}\text{Th})$	$(^{234}\text{U}/^{238}\text{U})_0$	Age Uncorrected (years BP)	Age Corrected (years BP)
KTR2 9	7	0.1778	0.1271	1.0209(12)	0.0636(32)	271.6	1.0213(12)	7033 ± 34	6947 ± 37
KTR2 8	35	0.2841	0.1985	1.0094(11)	0.0710(29)	309.9	1.0096(11)	7973 ± 32	7888 ± 35
KTR2 7	45	0.2290	0.2618	1.0065(11)	0.0745(35)	199.1	1.0066(11)	8419 ± 34	8321 ± 42
KTR2 6	58	0.1681	0.2714	1.0093(12)	0.0790(43)	149.7	1.0096(12)	8934 ± 38	8821 ± 50
KTR2 5	65	0.2173	0.2858	1.0029(12)	0.0770(36)	178.8	1.0030(11)	8746 ± 33	8641 ± 43
KTR2 4	96	0.1796	0.2306	1.0063(12)	0.0832(42)	197.9	1.0064(12)	9442 ± 43	9339 ± 50
KTR2 3	107	0.2575	0.8751	1.0082(12)	0.0933(69)	84.3	1.0084(12)	10,688 ± 41	10,522 ± 82
KTR2 2	118	0.2259	0.7026	1.0105(15)	0.1011(64)	99.7	1.0088(12)	11,585 ± 40	11,428 ± 76
KTR2 1	137	0.2147	5.4331	1.0308(36)	0.2232(42)	27.5	1.0332(38)	27,312 ± 930	26,514 ± 529

Table 3.

	Sample No	Lab. No	Conventional ¹⁴ C age (1σ) (radiocarbon years)	IntCal13 2σ calibration (cal. years BP)
Schinus fan F, roadside quarry				
Light-grey fine silt unit 10 cm above overlying palaeosol (sample MRL109914-5).	MRL090911-4	Beta-309118	4460±30	4970-5280
Upper 10 cm of prominent 30 cm thick light red palaeosol, 1.5 m above base of quarry floor.	MRL109914-5	Beta-150165	7620±40	8360-8440
Schinus fan F sea cliff section				
Impersistent light reddish brown palaeosol, 5.7 m above palaeosol sample JEA140916-5.	JEA140916-6	Beta-448200	4440±30	4890-5275
Light-grey fine silt unit, 10 cm above palaeosol sample JEA140916-5.	JEA140916-4	Beta-448198	7030±30	7795-7935
Prominent light reddish brown palaeosol horizon, 20 cm thick, 5.05 m above modern sea-level	JEA140916-5	Beta-448199	8660±30	9545-9680
Light brown palaeosol horizon, 20 cm thick, 2.0 m above modern sea-level	JEA140916-3	Beta-448197	8350±40	9280-9470

Highlights

Novel coupling of early Holocene stalagmite palaeoclimate record with timing of palaeosol development on nearby alluvial fan

New record of 8.2 ka palaeoclimate event in Greece

Alluvial fan palaeosol radiocarbon age aligns with documented climatic aridity ~8.2 ka

Palaeosol development was a non-random, allocyclic response, driven by climatic events.

Alluvial fan palaeosol formation ~8.2 ka may have been an allocyclic response to precipitation regime change.

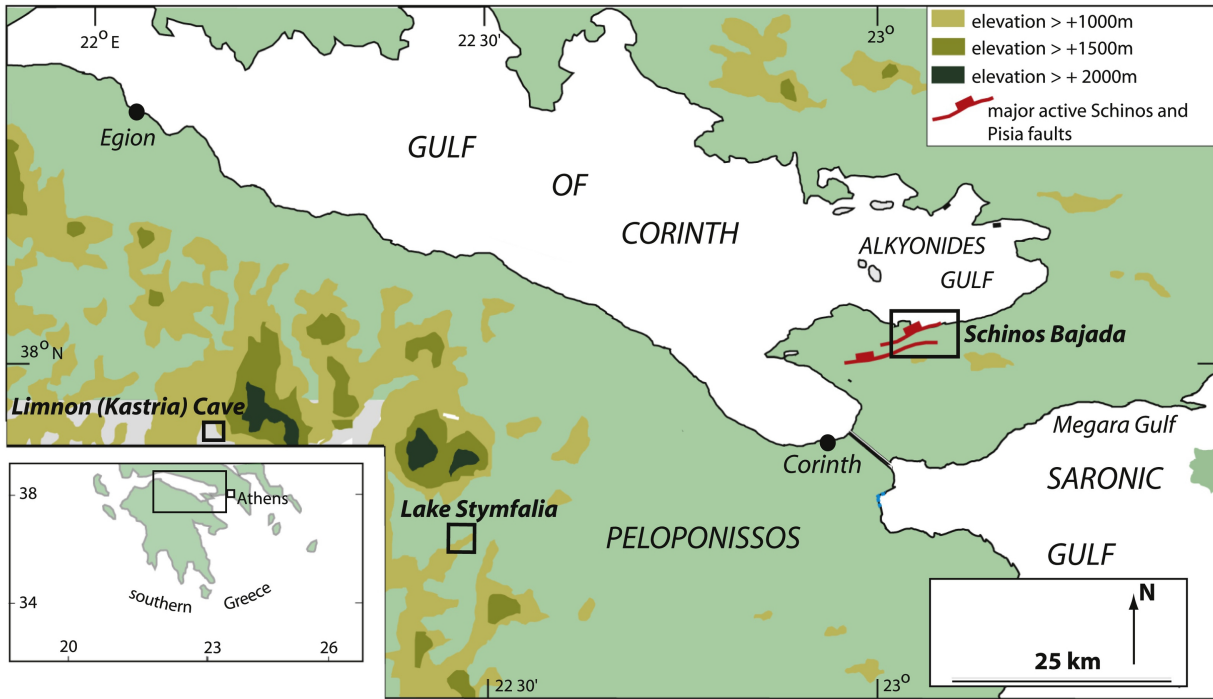


Figure 1

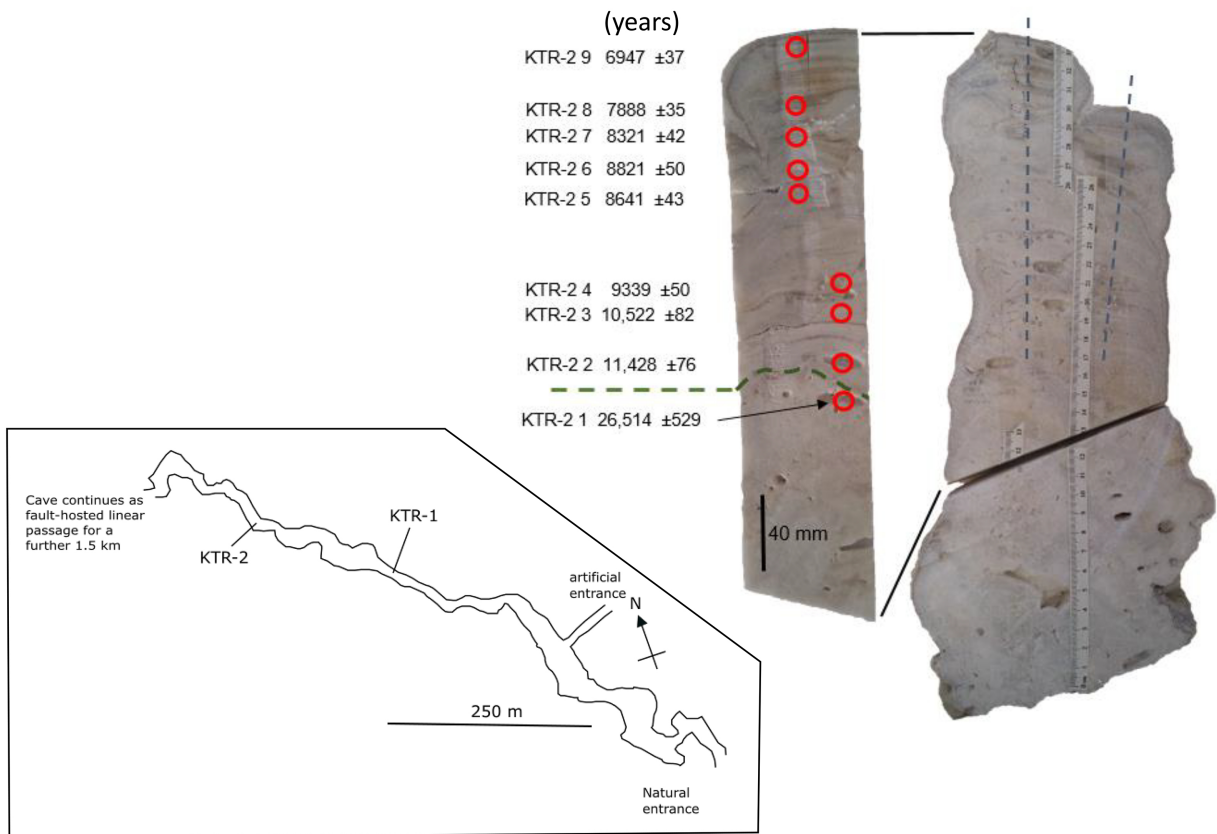


Figure 2

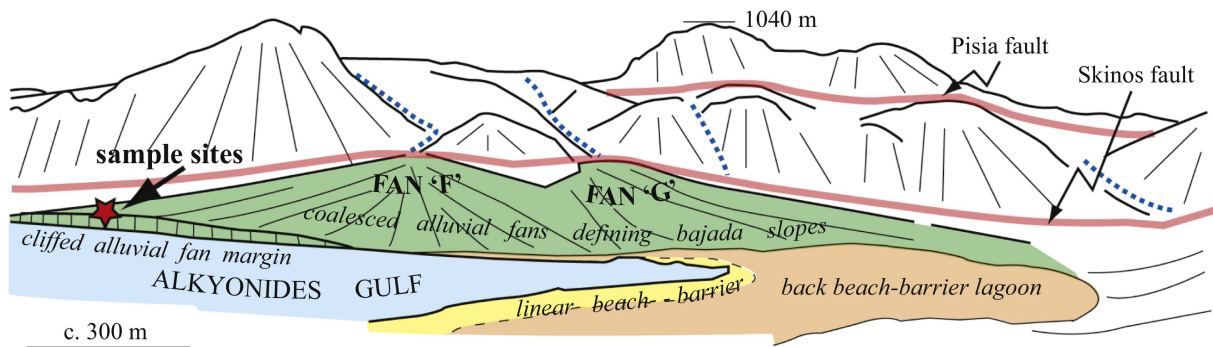


Figure 3

Limnon Cave StalAge Model

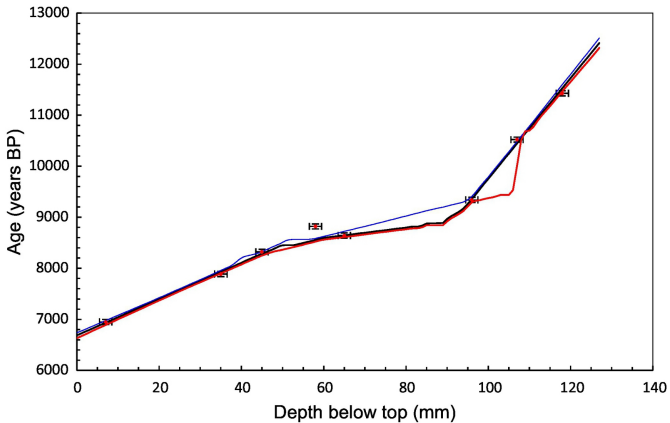


Figure 4

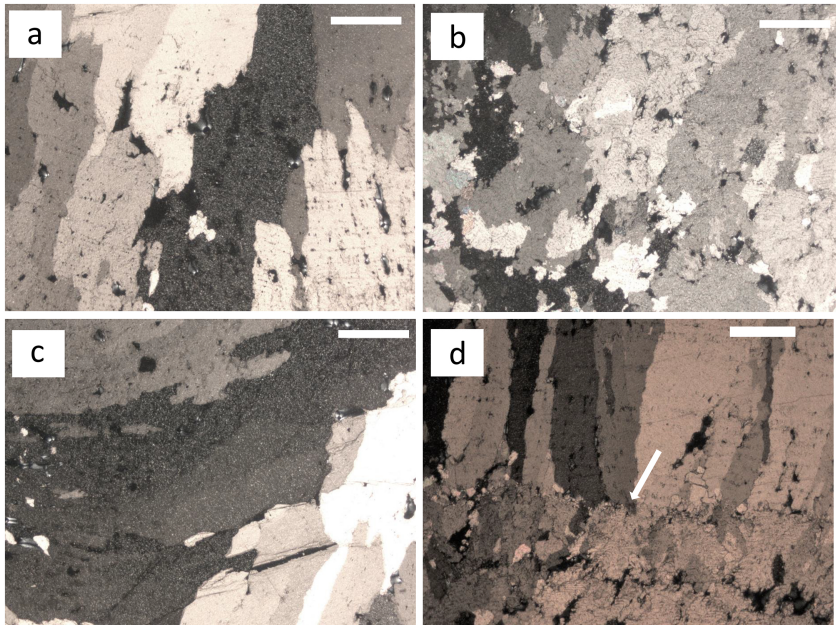


Figure 5

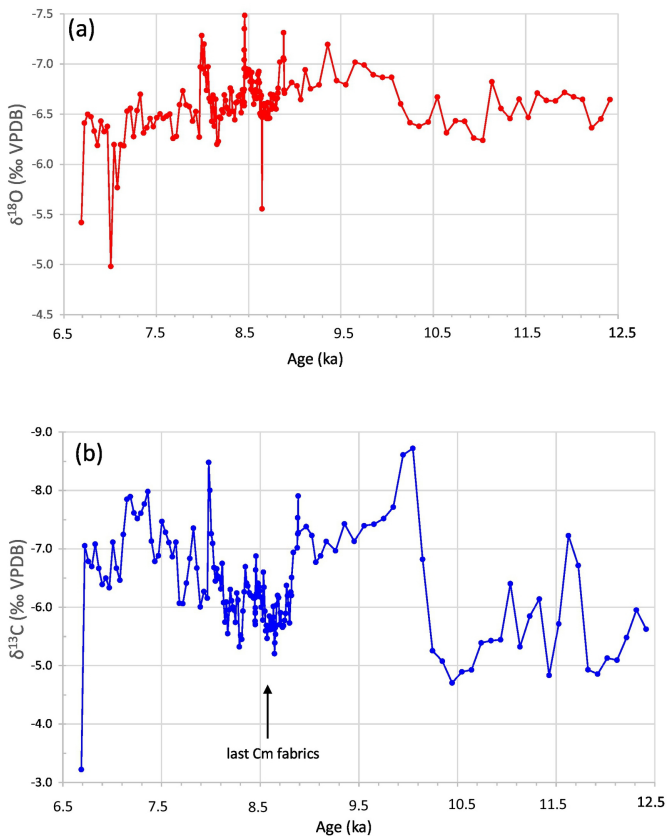


Figure 6

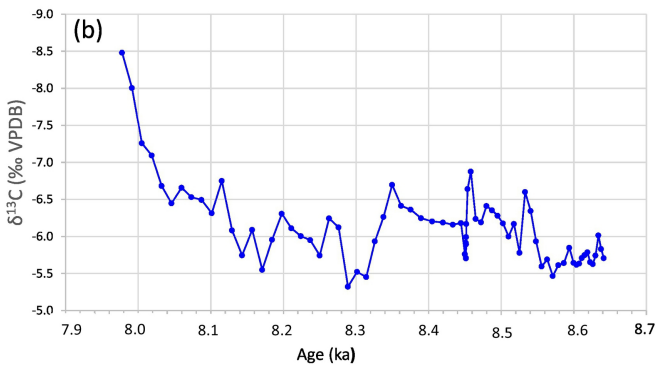
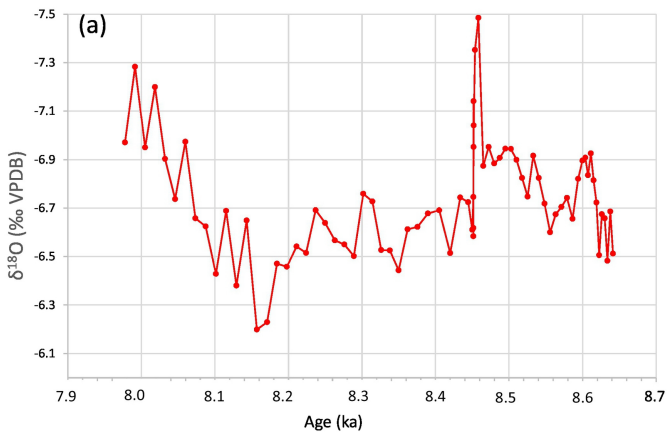


Figure 7

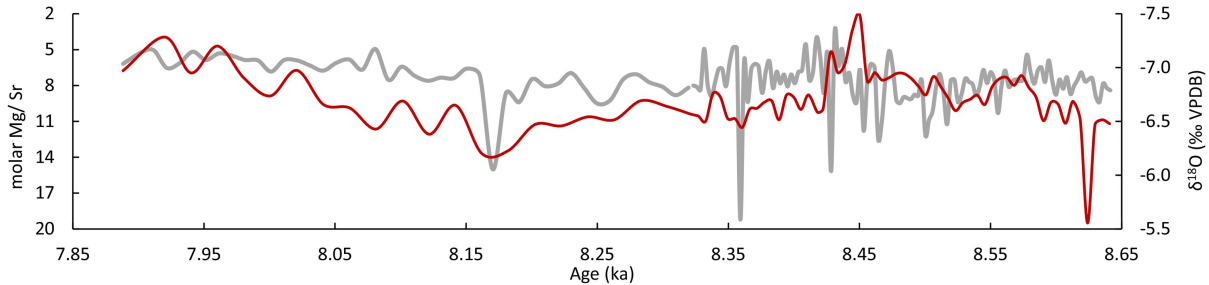
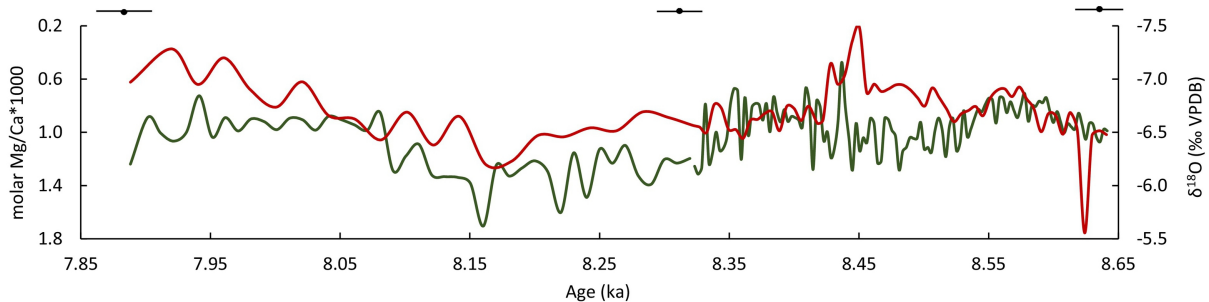


Figure 8



Figure 9

a



b



Figure 11

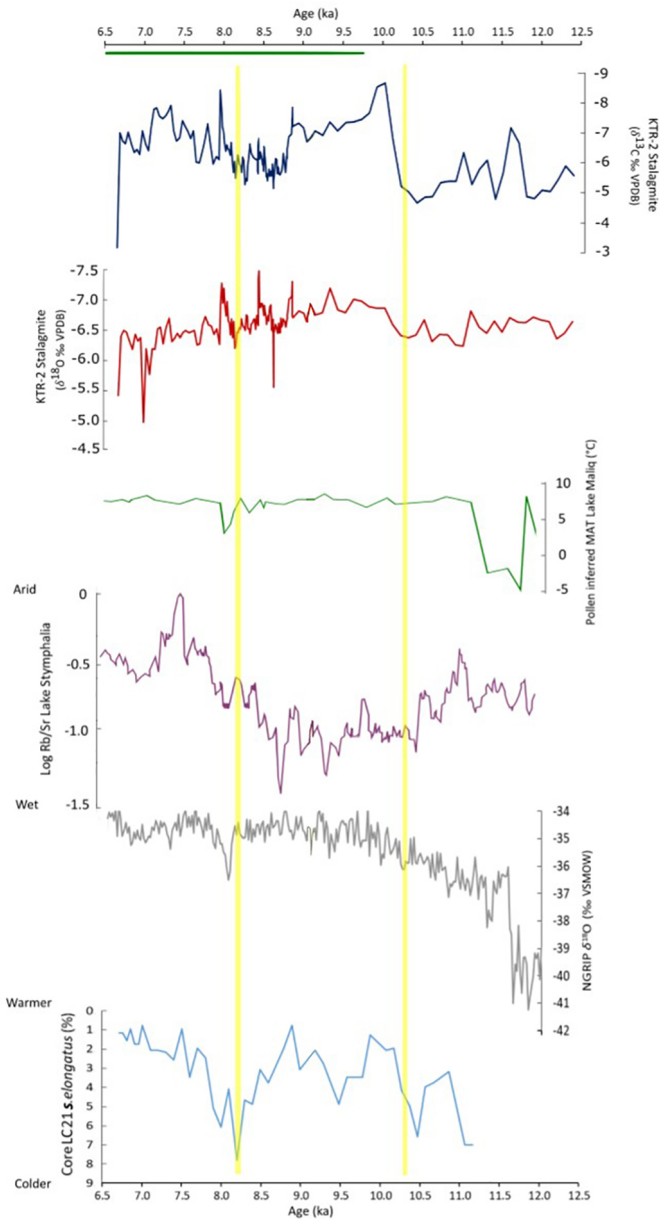


Figure 12

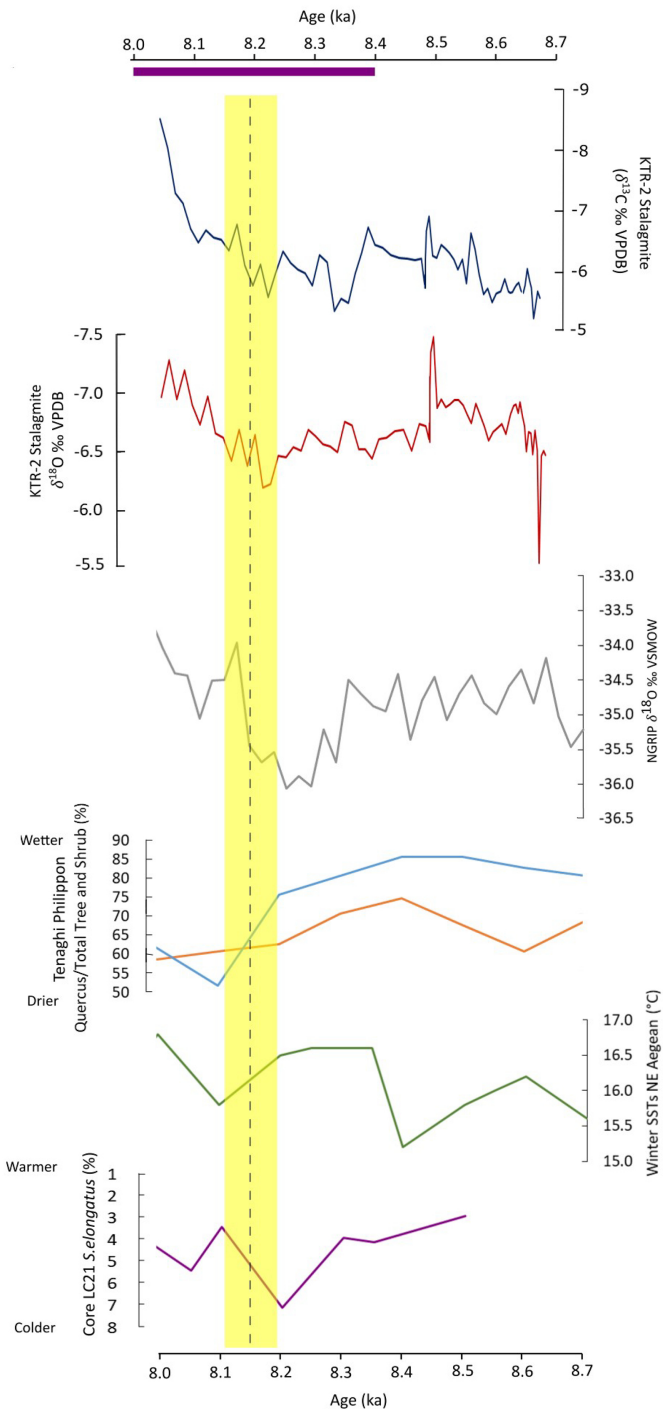


Figure 13